

Dynamic temperature selection for parallel-tempering in Markov chain Monte Carlo simulations

W. D. Vousden^{*}, W. M. Farr^{*} and I. Mandel^{*}

University of Birmingham, Edgbaston, Birmingham, B15 2TT, United Kingdom

16 March 2016

ABSTRACT

Modern problems in astronomical Bayesian inference require efficient methods for sampling from complex, high-dimensional, often multi-modal probability distributions. Most popular methods, such as Markov chain Monte Carlo sampling, perform poorly on strongly multi-modal probability distributions, rarely jumping between modes or settling on just one mode without finding others. Parallel tempering addresses this problem by sampling simultaneously with separate Markov chains from tempered versions of the target distribution with reduced contrast levels. Gaps between modes can be traversed at higher temperatures, while individual modes can be efficiently explored at lower temperatures. In this paper, we investigate how one might choose the ladder of temperatures to achieve more efficient sampling, as measured by the autocorrelation time of the sampler. In particular, we present a simple, easily-implemented algorithm for dynamically adapting the temperature configuration of a sampler while sampling. This algorithm dynamically adjusts the temperature spacing to achieve a uniform rate of exchanges between chains at neighbouring temperatures. We compare the algorithm to conventional geometric temperature configurations on a number of test distributions and on an astrophysical inference problem, reporting efficiency gains by a factor of 1.2–2.5 over a well-chosen geometric temperature configuration and by a factor of 1.5–5 over a poorly chosen configuration. On all of these problems a sampler using the dynamical adaptations to achieve uniform acceptance ratios between neighbouring chains outperforms one that does not.

1 INTRODUCTION

Many problems in astronomical data analysis and Bayesian statistical inference demand the characterisation of high-dimensional probability distributions with complicated structures. Lacking analytic forms, these distributions must be explored numerically, usually via Monte Carlo methods.

Parallel tempered Markov chain Monte Carlo (MCMC), a development on standard MCMC, uses several Markov chains in parallel to explore a target distribution at different “temperatures” (Earl & Deem 2005; Swendsen & Wang 1986; Geyer 1991). As the temperature increases, the posterior distribution asymptotes to the prior, allowing a chain to efficiently explore the whole prior volume without becoming stuck in regions of the parameter space with high probability density. At lower temperatures, a chain can more efficiently sample from such a high-probability region. Meanwhile, exchange of positions between chains allows colder chains to migrate between widely separated modes in the parameter

space (Geyer 1991). Parallel tempered MCMC samplers are thus particularly well-suited to sampling posterior distributions with well-separated modes, where a regular MCMC sampler would take many iterations to find its way between modes.

An open problem in the application of parallel tempering is selecting a specification, or ladder, of temperatures that minimises the autocorrelation time (ACT) of the chain sampling the posterior distribution of interest. The efficiency of a given ladder hinges critically on the rate at which it can transfer the positions in parameter space of samples between high and low temperatures.

In this paper we present a simple algorithm that adapts the temperature ladder of an ensemble-based parallel tempered MCMC sampler (Goodman & Weare 2010) such that the rate of exchange between chains is uniform over the entire ladder. The algorithm is easy to implement in existing code, and we provide an example implementation for the EMCEE sampler of Foreman-Mackey et al. (2013). We also present an implementation for traditional, non-ensemble MCMC samplers where a single walker explores

^{*} E-mail: will@star.sr.bham.ac.uk (WDV); w.farr@bham.ac.uk (WMF); imandel@star.sr.bham.ac.uk (IM)

the parameter space. We report favourable results from such an implementation, along with a number of caveats.

In [Section 2](#) we describe the parallel tempering formalism and lay out the requirements for a good temperature ladder. We discuss previous work on temperature selection and suggest a definition of ladder optimality that, for simple cases, proposes a geometric spacing of temperatures. For illustration, we apply these ideas in [Section 2.2](#) to the simple example of an unbounded Gaussian posterior distribution.

In [Section 3](#) we describe the algorithm mentioned above and then apply it in [Section 4](#) to a variety of test distributions. We show that, while our temperature selection strategy is not necessarily optimal in the ACT of the sampler, it nonetheless improves the ACT compared to the simple geometric spacing that is conventional in the literature ([Earl & Deem 2005](#); [Sugita & Okamoto 1999](#); [Kofke 2002, 2004](#)) by factors of > 1.2 for our test cases.

In [Section 5](#) we apply our method to the astrophysically motivated – and more challenging – problem of parameter estimation in the setting of gravitational wave (GW) data analysis, using a single-walker MCMC sampler. We demonstrate a reduction in ACT by as much as a factor of 2 over a geometric ladder, despite the caveats mentioned in [Section 6.1](#).

We conclude in [Section 6](#) with a discussion of our results and suggestions for further research.

2 PARALLEL TEMPERING

Parallel tempering ([Earl & Deem 2005](#); [Swendsen & Wang 1986](#); [Geyer 1991](#)) is a development on the standard MCMC formalism that uses several Markov chains in parallel to sample from tempered versions of the posterior distribution π ,

$$\pi_T(\vec{\theta}) \propto L(\vec{\theta})^{1/T} p(\vec{\theta}), \quad (1)$$

where L and p are respectively the likelihood and prior distributions.

For high T , individual peaks in L become flatter and broader, making the distribution easier to sample via MCMC. A set of N chains is assigned temperatures in a ladder $T_1 < T_2 < \dots < T_N$, with $T_1 = 1$ (the target temperature). The temperatures are typically geometrically spaced from 1 up to some T_{\max} , decided in advance (a convention that we shall discuss in more detail in [Section 2.2](#)).

Each chain is allowed to explore its tempered distribution π_T under an MCMC algorithm, while at pre-determined intervals “swaps” are proposed between (usually adjacent¹) pairs of chains and accepted with probability

$$A_{i,j} = \min \left\{ \left(\frac{L(\vec{\theta}_i)}{L(\vec{\theta}_j)} \right)^{\beta_j - \beta_i}, 1 \right\}, \quad (2)$$

where $\vec{\theta}_i$ is the current position in the parameter space of the i^{th} chain and $\beta_i \equiv 1/T_i$ is the inverse temperature of this chain. When a swap is accepted, the chains exchange

their positions in the parameter space, so that chain i is at $\vec{\theta}_j$ and chain j is at $\vec{\theta}_i$. Since the hottest chains can access all of the modes of π (as long as T_{\max} is chosen appropriately), their locations propagate to colder chains, ultimately allowing the $T = 1$ (cold) chain to efficiently explore the entire target distribution. At the same time, the positions of the colder chains propagate upward to higher temperature chains, where they are free to explore the entire prior volume.

The goal in choosing an effective ladder of temperatures is to minimise the ACT of the cold chain (our measure of the efficiency of the sampler). The requirements to this end are two-fold:

(i) T_{\max} must be large enough that isolated modes of L broaden sufficiently that an individual MCMC chain can efficiently access all of these modes when sampling under the tempered posterior π_T in (1) at $T = T_{\max}$. We denote this temperature T_{prior} .

(ii) Since $A_{i,j}$ depends on $\beta_i - \beta_j$, the differences between temperatures must be small enough that neighbouring chains can communicate their positions efficiently with one another.

Both requirements depend sensitively on the (unknown) shape of the target distribution, so it is difficult to select temperatures appropriately in advance.

In choosing T_{\max} , one must know roughly the relative size and separation of the modes to be explored. As an example, consider a one-dimensional likelihood with two Gaussian modes of width $\sigma = 1$ and centres $\mu = \pm 10$. In order to prevent a sampler from getting stuck on one of the modes, they must be widened to roughly the separation between them², giving $\sigma = O(10)$. The width of a Gaussian peak scales with the temperature as \sqrt{T} , so we might choose $T_{\max} = 100$; [Figure 1](#) illustrates the resulting coalescence of the modes. A different configuration of modes will, of course, require a different T_{\max} .

On the other hand, the swap acceptance probability $A_{i,j}$ depends on the distribution of likelihood values at temperatures T_i and T_j . In the case of a likelihood distribution comprising a single Gaussian mode, the time-averaged acceptance ratios between chains, $E[A_{i,j}]$, can be computed analytically (see [Section 2.2](#)).

In general, we don’t know in advance what the target distribution looks like, and so choosing an effective ladder becomes a heuristic exercise, relying largely on educated guesswork. We are therefore motivated to find some method of empirically determining an effective ladder.

2.1 Ladder selection

For an n -dimensional problem, the conventional choice of temperatures is a geometrically spaced ladder constructed so that approximately 23% of swaps proposed between chains will be accepted when sampling from an n -dimensional, unbounded Gaussian distribution ([Earl & Deem 2005](#); [ter](#)

¹ In principle, swaps can be proposed between any pair of chains. However, since the swap acceptance ratio (2) decays exponentially with the separation of inverse temperatures, $\Delta\beta$, it is generally sufficient only to propose swaps between adjacent chains.

² Ideally, the modes must also be widened enough that they extend to the edges of the prior volume. A likelihood distribution with a single mode that occupies only a small fraction of the prior volume will take a long time to burn in.

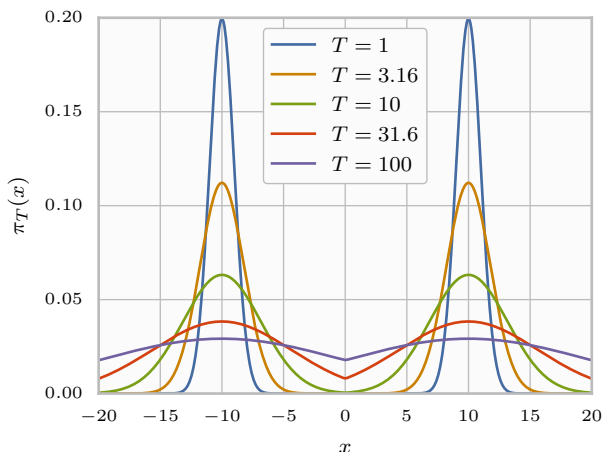


Figure 1. A one-dimensional target distribution with two Gaussian peaks of width $\sigma = 1$ at $\mu = \pm 10$ normalised for a uniform prior over $[-20, 20]$. At $T = 100$, the peaks broaden to $\sigma = 10$, allowing an MCMC chain sampling at this temperature to find both modes quickly, starting from anywhere within the prior volume.

Braak & Vrugt 2008; Roberts & Rosenthal 1998). We shall discuss this convention in more detail in Section 2.2.

A consequence of this strategy is that increasing the number of chains N does not improve communication between existing chains, which is determined by $E[A_{i,j}] = 0.23$. Instead, adding new chains extends the ladder to higher temperatures. This may be appropriate for an unbounded posterior, but for a realistic problem with a finite prior volume, the acceptance ratio between adjacent chains saturates to $\sim 100\%$ at some temperature T_{prior} , at which the posterior π_T begins to look like the prior p .

For this geometric spacing scheme – where T_{prior} is unknown – there is therefore an optimal number of chains, N_{opt} , such that $T_{\text{prior}} \approx T_{N_{\text{opt}}} \equiv T_{\text{max}}$. For $N < N_{\text{opt}}$ none of the chains will be sampling from the prior (so the sampler may not find all of the modes), while for $N > N_{\text{opt}}$ we end up with several chains sampling redundantly from the prior.

Since we are generally ignorant of T_{prior} for the problem at hand, we are motivated to find an alternative temperature selection strategy.

It has been suggested in the literature (Earl & Deem 2005; Sugita & Okamoto 1999; Kofke 2002, 2004) that one could select temperatures such that the acceptance ratios $A_{i,j}$ are uniform for all pairs (i, j) of adjacent chains, in an attempt to ensure that each sample sequence $\vec{\theta}(t)$ for $t = 1, 2, \dots$, as it moves between chains, spends an equal amount of time at every temperature. Sugita & Okamoto (1999) justify this notion experimentally – in the context of molecular dynamics – with test cases in which such a ladder indeed performs well. They use an algorithm derived from that of Hukushima & Nemoto (1996), which selects temperatures according to an iterative process for which a uniform- A ladder is a fixed point. Earl & Deem (2005) provide further references for similar methods of determining temperature ladders that yield a given a target acceptance ratio (Rathore et al. 2005; Sanbonmatsu & García 2002; Schug et al. 2004). However, these methods do not address

requirement (i), discussed above, that the temperature ladder should reach a T_{max} sufficient for all of the modes of L to mix (specified by T_{prior}).

Kofke (2002) discusses the selection of temperature ladders in the context of molecular simulations. He shows that, in simulations of such thermodynamic systems, there is a close relation between the specific heat of the system, C_V , and the acceptance ratios between adjacent temperatures. In particular, when C_V is constant with respect to T over a given temperature interval, then a geometric spacing of temperatures on that interval yields uniform acceptance ratios between adjacent temperatures.

In the language of thermodynamics, the energy of the system, U , is analogous to $-\log L$, and an analogue to the specific heat can therefore be defined as

$$C_V(T) = -\frac{d}{dT} E[\log L]_T, \quad (3)$$

where $E[\cdot]_T$ denotes the expectation operator over $\vec{\theta}$ under the distribution $\pi_T(\vec{\theta})$. $E[\log L]_T$ is therefore the expectation of the *untempered* log likelihood collected when sampling from the posterior at temperature T .

In the context of Bayesian inference, Kofke’s result therefore tells us that if the mean log likelihood collected by a sampler responds linearly to changes in temperature, then a geometrically spaced temperature ladder will achieve uniform acceptance ratios between adjacent chains. Conversely, temperature intervals on which $E[\log L]_T$ is strongly non-linear in T represent a phase transition that will require more careful placement of temperatures, as we shall show in Section 4.

2.2 The ideal Gaussian distribution: a simple example

In the simple case of a unimodal Gaussian likelihood under a flat prior, the optimal temperature spacing at low temperatures – where very little likelihood mass is truncated by the prior – can be analysed by approximating the prior to be unbounded³. We show that, for this tractable example, a geometric temperature spacing is consistent with both the uniform- A criterion and also with the alternative criterion that the Kullback–Leibler (KL) divergence is uniform between all pairs of adjacent chains. We use the example to illustrate the relationship between the analytical distribution of $\log L$, the acceptance ratio $A_{i,j}$, and the temperature T .

We shall work with an n -dimensional unit Gaussian centred on the origin (the same result can be achieved for a general Gaussian through a simple change of coordinates). Since the prior is uniform and unbounded, we can restrict attention to the likelihood distribution L . In this case, the probability density \tilde{p} for the values of $\log L(\vec{\theta})$ collected by the sampler is

$$\tilde{p}(\log L) = \frac{e^{\log L} (-\log L)^{\frac{n}{2}-1}}{\Gamma(\frac{n}{2})}, \quad (4)$$

³ The approximation breaks down at higher temperatures, where boundary effects become significant. Indeed, with no prior boundaries, there is no T_{prior} at which the mode is spread over the entire prior volume.

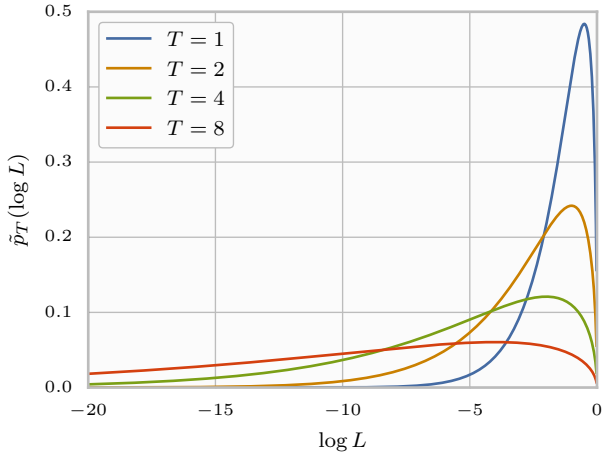


Figure 2. The distribution of $\log L$ under a three-dimensional, unimodal Gaussian at various temperatures, where L is normalised so that $\log L(\vec{0}) = 0$. As $T \rightarrow \infty$, the variance of $\log L$ diverges. The legend is ordered to match the vertical order of the lines' peaks.

where L is normalised so that $\log L(\vec{0}) = 0$ and n is the number of parameters.

At a temperature T , $-\log L$ simply follows a gamma distribution $\Gamma(\alpha, \beta)$ with shape parameter $\alpha = n/2$ and rate parameter $\beta = 1/T$. Thus, for a chain sampling at temperature T , the log likelihood distribution is $\tilde{p}_T(\log L) = T \tilde{p}(\log L/T)$.

Over long time-scales, the average acceptance ratio between chains i and j is

$$\begin{aligned} E[A_{i,j}] &= \iint_{(-\infty, 0]^2} A_{i,j} \tilde{p}_{T_i}(\log L_i) \tilde{p}_{T_j}(\log L_j) \, d\log L_i \, d\log L_j \\ &= \left(\frac{1}{\sqrt{\pi}} 2^{n-1} \gamma_{i,j}^{-n/2} \Gamma\left(\frac{n+1}{2}\right) \right) \\ &\quad \cdot \left({}_2\tilde{F}_1\left(\frac{n}{2}, n; \frac{n}{2} + 1; -\frac{1}{\gamma_{i,j}}\right) - \right. \\ &\quad \left. \gamma_{i,j}^n {}_2\tilde{F}_1\left(\frac{n}{2}, n; \frac{n}{2} + 1; -\gamma_{i,j}\right) \right) + 1, \end{aligned} \quad (5)$$

where ${}_2\tilde{F}_1$ is the regularised Gauss hypergeometric function and $\gamma_{i,j} = T_j/T_i$ is the ratio between the temperatures of two chains. Since $E[A_{i,j}]$ depends on T_i and T_j only through the ratio $\gamma_{i,j}$, uniform acceptance ratios between all adjacent pairs of chains can be achieved with a geometric spacing of temperatures – where $\gamma_{i,i+1}$ is constant – for a unimodal Gaussian likelihood.

The log spacing required for a particular acceptance ratio also depends on the dimension of the parameter space, with more parameters requiring a closer spacing of temperatures, illustrated by Figure 3. This can be understood by looking at the expectation and variance of $\log L$ at a particular temperature (see Figure 2),

$$E[\log L]_T = -\frac{nT}{2} \quad \text{and} \quad \text{Var}[\log L]_T = \frac{nT^2}{2}. \quad (6)$$

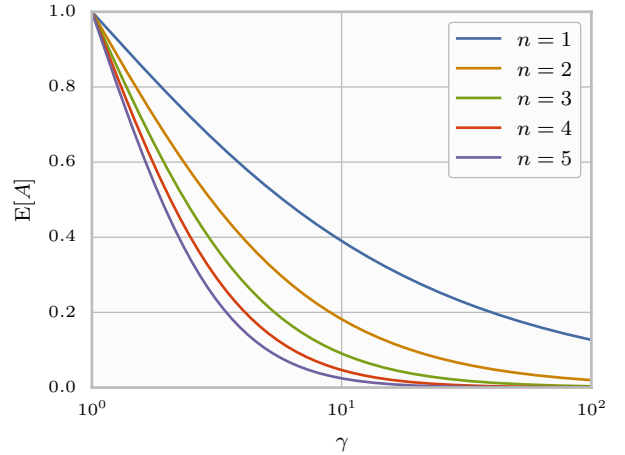


Figure 3. The time-averaged acceptance ratio, $E[A]$, between two chains of a PTMCMC sampler on a unimodal, n -dimensional Gaussian likelihood distribution. The chains have temperatures T and γT . The lines are ordered vertically to match the legend.

Note that the specific heat from (3) is a constant $n/2$, as expected.

Since the acceptance ratio $A_{i,j}$ depends on $\log L_i - \log L_j$, the more separate the distributions of $\log L_i$ and $\log L_j$ at their respective temperatures, T_i and T_j , the lower the acceptance ratio between such chains will be. For two chains at temperatures T and γT , the separation of the means of \tilde{p}_T and $\tilde{p}_{\gamma T}$, in units of the standard deviation at T , will be

$$\frac{E[\log L]_T - E[\log L]_{\gamma T}}{\sqrt{\text{Var}[\log L]_T}} = (\gamma - 1) \sqrt{\frac{n}{2}}. \quad (7)$$

It follows that – for constant γ – as the dimension n increases, so the acceptance ratio between chains at temperatures T and γT falls. For a higher dimensional target distribution, therefore, a closer spacing of temperatures is required for a given acceptance ratio.

For more general distributions, by considering the overlap of $\tilde{p}_T(\log L)$ at different temperatures, Falcioni & Deem (1999) argue that the number of temperatures N required to efficiently sample the posterior distribution should scale with $\Delta \log L / \sqrt{n}$, where $\Delta \log L$ is the range of $E[\log L]_T$ between $T = 1$ and $T = T_{\text{prior}}$. That is:

$$N \propto \frac{E[\log L]_1 - E[\log L]_{T_{\text{prior}}}}{\sqrt{n}}. \quad (8)$$

Since the log likelihood range $\Delta \log L$ itself depends on the dimension of the system n , it is difficult to apply this relation in practice. However, for the ideal Gaussian, we can see from (6) that $\Delta \log L$ scales with n , and so N scales with \sqrt{n} , as we might expect.

2.3 The Kullback–Leibler divergence

Another measure of the optimal spacing of temperatures is the Kullback–Leibler (KL) divergence between adjacent chains. The KL divergence from a hot distribution π_{T_j} to a

cold distribution π_{T_i} ,

$$D_{\text{KL}}(\pi_{T_i} \parallel \pi_{T_j}) = \int \pi_{T_i}(\vec{\theta}) \log \frac{\pi_{T_i}(\vec{\theta})}{\pi_{T_j}(\vec{\theta})} d\vec{\theta}, \quad (9)$$

quantifies the information gained about the posterior with each step down the temperature ladder, from the prior $p = \pi_{T=\infty}$ to the posterior $\pi = \pi_{T=1}$. It is reasonable to expect that for an optimally-spaced ladder – that is, one with a minimal ACT on the cold chain for a given number of chains – the information gain should be uniform for every step down the ladder.

For the example of the ideal Gaussian of Section 2.2, the KL divergence is, straightforwardly,

$$D_{\text{KL}}(\pi_{T_i} \parallel \pi_{T_j}) = \frac{n}{2} \left(\frac{1}{\gamma_{i,j}} + \log \gamma_{i,j} - 1 \right). \quad (10)$$

Like the swap acceptance ratio, therefore, uniform KL divergence over the entire ladder is also achieved by a geometric spacing of temperatures for the ideal Gaussian.

Unfortunately, unlike the acceptance ratio, the KL divergence is difficult to compute numerically while sampling, owing to the unknown – and temperature-dependent – evidence (normalisation) values on π_{T_i} and π_{T_j} .

We henceforth assume that spacing temperatures for uniform acceptance ratios is a reasonable approximation of a ladder that is optimal in the ACT of the cold chain. We make this assumption on faith and, while we briefly examine its validity in Section 4.1 and Section 6.1, it invites a more careful study.

3 ADAPTIVE TEMPERATURE LADDERS

From the arguments in Section 2 and the references therein, we shall assume that uniformity of acceptance ratios provides a good approximation to the optimal temperature ladder for parallel tempering problems. In this section, we describe an algorithm for dynamically adapting chain temperatures to achieve uniform acceptance ratios for inter-chain swaps.

From (2), as $1/T_j - 1/T_i \rightarrow 0$, $A_{i,j} \rightarrow 1$, so in order to increase the expected acceptance ratio between chains, it suffices to move them closer together in temperature space; conversely, to reduce $E[A_{i,j}]$, we can push the chains apart. We will henceforth adopt the notation that $A_i \equiv A_{i,i-1}$ and that $T_i < T_{i+1}$, with $T_1 = 1$ being the untempered or cold chain (which samples from the target distribution, π). Here, $A_i(t)$ are the instantaneous acceptance ratios between chains, but we shall shortly describe the discrete case where empirical measurements of A_i are collected with each iteration of the sampler.

3.1 Dynamics

Our goal is to dynamically adjust the temperatures of the chains to achieve uniform acceptance ratios as we sample the target distribution. We define our temperature dynamics in terms of the log of the temperature difference between chains,

$$S_i \equiv \log(T_i - T_{i-1}). \quad (11)$$

Under this scheme, finite changes to S_i will always preserve the correct ordering of temperatures ($T_1 < \dots < T_N$).

To achieve the same A_i for all chains, we can drive the gap S_i according to the acceptance ratios between chain i and those immediately above and below, to wit

$$\frac{dS_i}{dt} = \kappa(t) [A_i(t) - A_{i+1}(t)], \quad (12)$$

for $1 < i < N$, where κ is a positive constant controlling the time-scale of the evolution of T_i . κ can be interpreted as the instantaneous exponential time-constant for temperature adjustments. The two extremal temperatures, T_1 and T_N , are fixed (see below).

Under this scheme, chain i will attempt to increase the gap in temperature space between itself and chain $(i+1)$ if swaps are accepted too often and close it when they are accepted too seldom – and similarly for chain $(i-1)$ – equilibrating at A_i that are uniform over i . Therefore, for an appropriate choice of κ – discussed momentarily – these rules drive the chains $i = \{2, \dots, N-1\}$ toward even acceptance spacing.

However, in order to efficiently sample a target distribution with strongly separated modes (such that a traditional MCMC sampler would be unable to traverse the “valleys” between them), T_N must be high enough that the modes are flattened out and the chain can explore the entire parameter space unhindered. This amounts to the topmost chain sampling from the prior distribution⁴, which we achieve trivially by setting the inverse temperature of this chain as $\beta_N = 0$.

This continuous system is discretised as

$$S_i(t+1) - S_i(t) = \kappa(t) [A_i(t) - A_{i+1}(t)], \quad (13)$$

where $A_i(t)$ are the acceptance ratios accumulated by the sampler at the current iteration.

The values of A_i are measured empirically at each iteration as the fraction of swap proposals between chains that were accepted. For a traditional sampler comprising one sample per chain, these will be either 0 or 1. For ensemble samplers, however, comprising n_w distinct walkers per temperature, the measurements of A_i are less granular, such that $A_i \in \{x \in [0, 1] | n_w x \in \mathbb{Z}\}$. In general, fewer walkers require a longer averaging time-scale – discussed below – in order to smooth out this granularity.

Importantly, the temperature adjustment scheme we have proposed – and, more generally, any adaptive sampling scheme – in fact violates the condition for detailed balance that ensures that an MCMC sampler will converge to the target distribution. Roberts & Rosenthal (2007) investigate the conditions required of such an adaptive sampler for it to be ergodic in the target distribution – that is, that it will converge on long time-scales. They determine (from their Theorem 1 and Corollary 4) that diminishing the amplitude of adaptations in the transition kernel with each iteration is sufficient for the sampler to be ergodic in the target distribution. We therefore suppress temperature adjustments to ensure that the sampler is Markovian on sufficiently long time-scales⁵.

The rate of diminution of temperature adjustments is a

⁴ For analytic priors, this special case, where the likelihood is ignored, can be treated separately by having the sampler draw independent samples directly from the prior.

⁵ In principle, of course, we could stop temperature adjustments

trade-off between the rate of convergence of the temperature ladder and that of the sampler itself toward its stationary distribution. We modulate the dynamics with hyperbolic decay to suppress the dynamics on long time-scales,

$$\kappa(t) = \frac{1}{\nu} \frac{t_0}{t + t_0}, \quad (14)$$

where t_0 is the time at which the temperature adjustments have been reduced to half their initial amplitude. The initial amplitude of adjustments is in turn set by ν , the time-scale on which the temperatures evolve at early time.

3.2 Parameter choice

In the scheme of (13) and (14), there are two parameters to choose: t_0 and ν . The dynamical time parameter t in (13) is measured in units of intra-chain jumps of the sampler, with temperature adjustments being made at every iteration.

The lag parameter t_0 sets the time-scale for the attenuation of temperature adjustments. This decay factor in κ is included as a fail-safe mechanism to ensure that, even for target distributions on which the temperature dynamics fail to find an equilibrium set of temperatures, the ladder will always converge over long time-scales. This condition guarantees that the sampler correctly explores the target distribution.

From (14), the time-scale of the dynamics at late time – when $t \gg t_0$ – is $\nu t/t_0$. To ensure that temperatures have time to find an equilibrium over the course of a run, we therefore require that $t_0 \gg \nu$, so that the dynamics will always be on a time-scale much shorter than the current run time. However, we should also ensure that, over the course of the run, the dynamical time-scale is *longer* than the ACT of the sampler, so that the temperatures respond to the correct posterior distribution. To this end, we require that $\nu N_\tau \gg t_0$, where N_τ is the number of independent samples gathered over the course of the run. For example, if $N_\tau = 100$, these two conditions are satisfied by $t_0 = 10\nu$, and for our test cases, we have indeed found this choice to work well.

Meanwhile, the time-scale of the dynamics at early time – when $t \ll t_0$ – is ν . A good choice of ν should therefore ensure that the sampler is not susceptible to large statistical errors on the measurements of the acceptance ratios A_i .

In general, for n_s swap proposals, the acceptance count $n_s A_i$ is a random variable that follows a binomial distribution $B(n_s, E[A_i])$, so that A_i has variance

$$\text{Var}[A_i] = \frac{E[A_i](1 - E[A_i])}{n_s}.$$

Since the dynamical equations (13) are linear in A_i , they will be driven by the means, $E[A_i]$, on long time-scales, assuming that the noise in the system from counting errors – proportional to $1/\sqrt{n_s}$ – does not cause short-term changes in $E[A_i]$.

Given a sampler of n_w walkers, n_w swaps are proposed with each iteration, so that $n_s = n_w \nu$. To ensure stable dynamics at early time, we should therefore choose $n_w \nu \gg 1$.

altogether once the temperatures have reached an equilibrium, discarding the previous samples as part of the burn-in.

A good choice of ν depends on the response of $E[A_i]$ to changes in the relevant chains' temperatures, and therefore depends on the particular likelihood function that is being sampled. However, if $E[A_i]$ will eventually be of order, say, 0.25, and we want the measurements of A_i to be between 0.2 and 0.3, then we should average A_i over at least 100 swap proposals, giving $\nu \gtrsim 100/n_w$.

Combining these criteria on ν and t_0 , we therefore suggest default parameter values of $\nu = 10^2/n_w$ and $t_0 = 10^3/n_w$.

4 EXAMPLES

We have implemented the algorithm proposed above as a modification to the ensemble sampler EMCEE of [Foreman-Mackey et al. \(2013\)](#). Our implementation can be found at <https://github.com/willvousden/ptemcee>.

In this section we apply our implementation to specific examples in order to understand how and when the traditional geometric spacing fails and how much the uniform- A strategy might help us. We present the following test cases.

(i) In [Section 4.1](#) we compare the uniform- A strategy used by the temperature dynamics of [Section 3](#) with the alternative strategy of uniform KL divergence discussed in [Section 2.2](#) on the example of a unimodal truncated Gaussian likelihood.

(ii) In [Section 4.2](#) we test the dynamics on a more complex, bimodal distribution for various choices of the number of chains N . We compare the resulting ACTs of the sampler with those of another sampler using a geometric ladder whose maximum temperature is fixed such that $T_{\max} \approx T_{\text{prior}}$.

(iii) In [Section 4.3](#) we test the algorithm against the more difficult egg-box distribution with 243 modes. For comparison, we sample from the same distribution with a geometric ladder constructed to yield 25% acceptance ratios when applied to the ideal Gaussian discussed in [Section 2.2](#).

For all of these tests, $\nu = 10^2$ and $t_0 = 10^3$ are used to control the dynamics in (14), while the sampler uses 100 walkers. Note that these choices, while different from the defaults proposed in [Section 3.2](#), do satisfy the conditions described in that section.

4.1 Truncated Gaussian

Our first test case is an n -dimensional, unimodal, unit Gaussian similar to that of [Section 2.2](#) but with finite prior volume. The simplicity of this case admits some exact analysis before recourse to numerics, which allows us to test the approximations made in [Section 2.2](#).

At low temperatures, where the prior boundaries do not truncate much of the likelihood probability mass, the optimal temperature spacing should be similar to that of the ideal Gaussian. By imposing a step-like cut-off in the prior at a radius of R , there will be some temperature at which this approximation will fail and a geometric spacing becomes inappropriate.

For the likelihood we use the same distribution as in [Section 2.2](#), while for the prior we use a uniform distribution

over the closed n -ball of radius $R = 30$, centred on the origin. The likelihood and prior are defined by

$$L(\vec{\theta}) \propto \exp\left(-\frac{1}{2} \|\vec{\theta}\|^2\right), \quad (15)$$

$$p(\vec{\theta}) \propto \begin{cases} 1 & \text{if } \|\vec{\theta}\| \leq R, \\ 0 & \text{otherwise,} \end{cases} \quad (16)$$

where $\|\cdot\|$ is the Euclidean norm on \mathbb{R}^n . Subsequently, the normalised posterior generated by (15) and (16) at temperature T is

$$\pi_T(\vec{\theta}) = \begin{cases} \frac{(2\pi T)^{-\frac{n}{2}} \Gamma(\frac{n}{2})}{\tilde{\gamma}(\frac{n}{2}, \frac{R^2}{2T})} \exp\left(-\frac{\|\vec{\theta}\|^2}{2T}\right) & \text{if } \|\vec{\theta}\| \leq R, \\ 0 & \text{otherwise,} \end{cases} \quad (17)$$

where $\tilde{\gamma}(a, z)$ is the lower incomplete gamma function.

In the low-temperature limit, this distribution converges to the ideal Gaussian distribution. We should therefore expect the KL divergence for a step down the temperature ladder to asymptote to (10) as $T \rightarrow 0$, where the effects of the prior boundary are negligible⁶. Indeed, the KL divergence of (17) from T_2 to T_1 is available analytically as

$$D_{\text{KL}} = -\frac{(T_2 - T_1) \tilde{\gamma}\left(1 + \frac{n}{2}, \frac{R^2}{2T_2}\right)}{T_2 \tilde{\gamma}\left(\frac{n}{2}, \frac{R^2}{2T_1}\right)} + \frac{n}{2} \log\left(\frac{T_2}{T_1}\right) + \log\left(\frac{\tilde{\gamma}\left(\frac{n}{2}, \frac{R^2}{2T_2}\right)}{\tilde{\gamma}\left(\frac{n}{2}, \frac{R^2}{2T_1}\right)}\right). \quad (18)$$

If we set $T_2 = \gamma T_1$ (with $\gamma T_1 \ll 1$), then $\tilde{\gamma}(a, z) \rightarrow \Gamma(a)$ as $T_1 \rightarrow 0$, and the expression reduces to (10), as expected.

Figure 4 illustrates this convergence for $n = 5$. The point on this plot at which the solid line diverges from the dashed line, for each γ , predicts the temperature beyond which a geometric spacing of temperatures is no longer optimal (for optimality as defined by uniform KL divergence between chains). This is caused by truncation of the tempered likelihood by the prior boundaries.

Of course, since the KL divergence cannot easily be assessed empirically by an MCMC sampler, and we must instead resort to using acceptance ratios, we would like to know how consistent these two schemes are outside the assumptions of Section 2.2.

Figure 5 shows contours of constant D_{KL} , calculated from (18), and contours of constant A_i , illustrated by points representing temperature pairs (from ladders selected by the algorithm developed in Section 3). In the low temperature limit, as expected, both schemes select a geometric spacing of temperatures consistent with the ideal Gaussian of Section 2.2 (i.e., the contours remain constant in γ). At higher temperatures, both schemes depart from the geometric spacing, but they do so differently. The uniform acceptance scheme displays a more gradual departure from a geometric spacing than the contours of constant D_{KL} . The smaller γ selected by the uniform- A scheme outside the geometric regime, however, suggest that closer spacing is required in difficult temperature ranges (e.g., across a phase

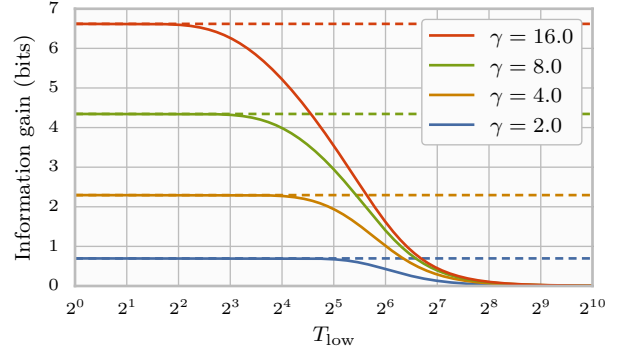


Figure 4. The KL divergence, or information gain, from a hot chain at temperature γT_{low} to a colder chain at temperature T_{low} , both sampling from (17) at $n = 5$ (solid lines). As $T_{\text{low}} \rightarrow 0$, the information gain tends to that of the ideal Gaussian of Section 2.2 (dashed lines). The lines are ordered vertically to match the legend.

transition) in order to achieve uniform A than would be required for uniform D_{KL} . There is therefore less risk of a large gap in temperature across such a temperature range, at the cost of (potentially) slightly less efficient communication across the rest of the ladder. The uniform- A criterion for optimality is therefore conservative with respect to a uniform- D_{KL} criterion.

We can also visualise the ladder specification in terms of the density of chains over temperature. We define this density, in $\log T$, as

$$\eta(\log T) = \frac{dN}{d \log T} = \frac{1}{\Delta \log T} = \frac{1}{\log \gamma}, \quad (19)$$

with $\gamma = T_{i+1}/T_i$, where T_{i+1} and T_i are the chain temperatures to either side of T .

Figure 6 shows this density for a temperature ladder of 20 chains that is in equilibrium under the temperature dynamics of Section 3 (the $N = 20$ contour of Figure 5). The density exhibits the expected uniformity of γ for low temperatures but falls for $T \gtrsim 80$. The width σ of the unit Gaussian at temperature T is \sqrt{T} , so at this temperature the prior boundary is at $\sim 3\sigma$. At $T = 80$, $\sim 5\%$ of the likelihood mass is truncated – compared to $< 0.1\%$ for $T = 40$ and $\sim 35\%$ for $T = 160$ – indicating that the prior boundary becomes significant in this temperature regime.

This drop in density reflects the convergence of the tempered posterior distribution, π_T , toward the prior as $T \rightarrow \infty$. As π_T becomes flatter, fewer chains are needed per $\log T$ to maintain good communication.

Also shown on figure Figure 6 is the square root of the estimated specific heat C_V of the system as discussed in Section 2.1, which can be seen to track closely the logarithmic chain density η when appropriately normalised. While the provenance of this relationship is unclear, it demonstrates the relevance of the specific heat in determining an effective temperature ladder.

⁶ While we do not consider $T < 1$ in our simulations, the case of $T \rightarrow 0$ can equivalently be thought of as $R \rightarrow \infty$, since the width of the Gaussian scales with \sqrt{T} .

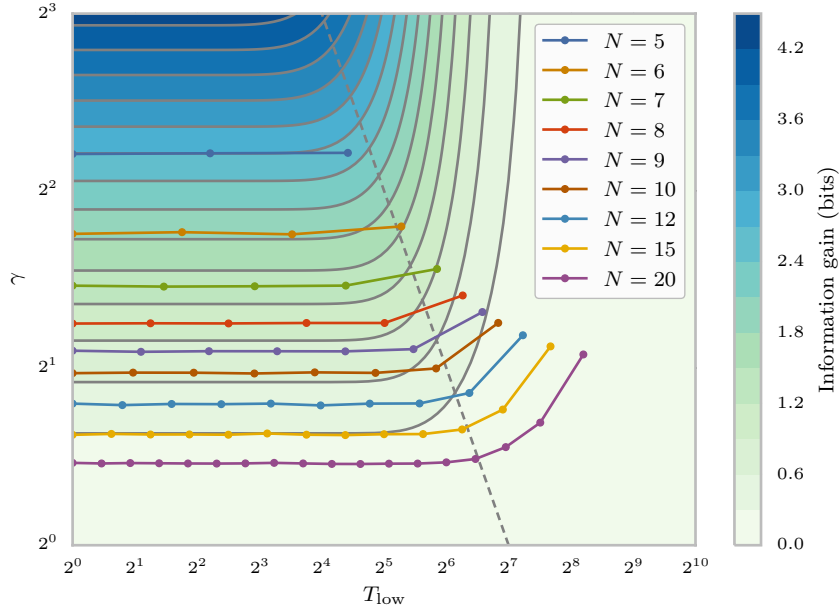


Figure 5. A contour plot of the KL divergence, or information gain, from a hot chain at temperature $T_{\text{high}} = \gamma T_{\text{low}}$ to a colder chain at temperature T_{low} , both sampling from the Gaussian likelihood (17). The coloured lines show the equilibrium N -chain temperature ladders reached by the temperature dynamics algorithm of Section 3, where the acceptance ratio is the same between any pair of adjacent chains. The points on these lines represent pairs of adjacent temperatures $(T, \gamma T)$ (excluding the top-most, where $\gamma = \infty$).

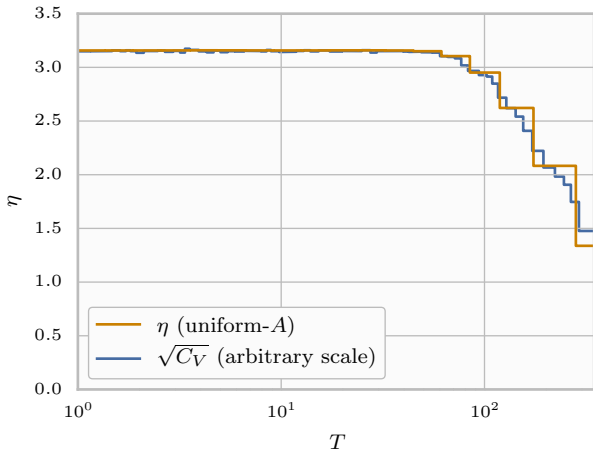


Figure 6. **Orange:** The density of chains per $\log T$ under the truncated Gaussian distribution (17), where $N = 20$, $n = 25$, and temperatures are chosen for uniform acceptance ratios between chains. The chains have equilibrated to 77% acceptance. **Blue:** The square root of the specific heat of the truncated Gaussian distribution, normalised to match the chain density η of the uniform- A ladder, between T_1 and T_{N-1} . The specific heat C_V , from (3), is estimated from the sample means of $\log L$ over many runs with different temperature ladders.

4.2 Double Rosenbrock function

The previous test demonstrated how a geometric ladder spaces temperatures too closely at higher temperatures, as the prior boundary becomes significant. While this may be

an inefficient use of resources, it at least doesn't drastically inhibit communication between high temperatures and low temperatures. Instead, we now turn to a more complex, bimodal likelihood distribution for which a geometric spacing might cause bottlenecks in the communication between high and low temperatures.

We use a likelihood derived from the two-dimensional Rosenbrock function f :

$$L(x, y) \propto \left(\frac{1}{c + f(x, y)} + \frac{1}{c + f(-x, y)} \right)^{1/T_p}, \quad (20)$$

where

$$f(x, y) = (a - x)^2 + b(y - x^2)^2. \quad (21)$$

T_p is a pre-tempering factor chosen to increase the contrast of the distribution, making it harder to sample. When $T_p \ll 1$, each mode is locally Gaussian, making the results comparable to the Gaussian example considered in Section 2.2.

For the following tests, we use $a = 4$, $b = 1$, $c = 0.1$, and $T_p = 10^{-3}$. We use a flat prior on $[-10, 10] \times [-20, 100]$. Figure 7 illustrates this likelihood over the prior volume.

4.2.1 Test: temperature evolution

As an illustrative example, we first tested the temperature dynamics of Section 3 with the double Rosenbrock posterior distribution (20) using 13 chains. Figure 8 shows the evolution of the temperature ladder according to these dynamics, while Figure 9 shows the chain density $\eta(\log T)$ for the equilibrated temperature ladder.

While the equilibrated chains are distributed uniformly in $\log T$ for $T \lesssim 50$, there is a distinct peak in η at $T \approx 800$,

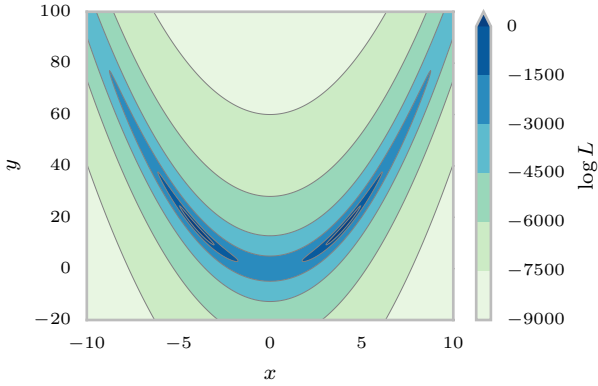


Figure 7. The Rosenbrock log likelihood, from (20).

where a simple geometric spacing of temperatures hinders communication between chains. This peak occurs at a phase transition where the two modes of the likelihood distribution begin to mix and $E[\log L]$ changes rapidly with T , indicated by the sharp change in specific heat in the bottom panel of Figure 9. Since the shape of the likelihood distribution in this regime becomes very sensitive to T , a higher density of chains is needed to maintain a given acceptance ratio. We also note that in the geometric regime (i.e., for low T) the specific heat is approximately $n/2 = 1$, with $E[A] \approx 57\%$, consistent with the values derived for the ideal Gaussian from (6) and (5) respectively.

Ultimately, however, the figure of merit for a temperature specification in a PTMCMC simulation is the resulting ACT for the target temperature ($T = 1$) of the sampler. We must therefore test the performance of the sampler empirically.

We use the term ACT to refer to the *integrated autocorrelation time* discussed by Sokal (1997), which we estimate according to the algorithm used in the *acor* package (see Appendix A and <http://www.math.nyu.edu/faculty/goodman/software/acor/> for details). For the following tests, we use the ACT of the first parameter, x , as a measure of the efficiency of the sampler (since (20) is bimodal in x but unimodal in y).

4.2.2 Test: improvement over a geometric ladder

In Section 2 we claimed that aiming for uniform acceptance ratios between chains yields a good temperature ladder. Specifically, we expect that a ladder selected for uniform acceptance ratios should lead to a lower ACT for the $T = 1$ chain than that resulting from a plain geometric ladder.

The geometric ansatz that we use has a fixed maximum temperature such that $T_N = 2 \times 10^4$. As N increases, more chains are added between T_1 and T_N , maintaining the geometric spacing. Under this arrangement, the addition of new temperatures is not redundant even when T_N is already high enough to sample from the prior; the additional chains instead aid inter-chain communication at lower temperatures. Since T_N is close to the temperature at which the posterior becomes the prior, there is little CPU time wasted in sampling redundantly from the prior with several chains, while

lower-temperature chains can still communicate with a chain sampling from the prior. Under this set-up, therefore, the ACT always decreases as N increases, per Figure 10.

To test the improvement in ACT, τ , conferred by our temperature dynamics, we allowed EMCEE to explore the target distribution (20) with different numbers of chains, N , using both the uniform- A ladders and geometrically spaced ladders. The resulting ACTs, τ_{geo} and τ_{acc} , are plotted against N in Figure 10.

In this example, an N -chain ladder dynamically adapted for uniform acceptance ratios clearly outperforms a geometrically spaced ladder of the same size for all N .

The benefit of a uniform- A ladder is most pronounced at low N – i.e., where there are few chains available. In this regime, the sampler will be more sensitive to phase transitions, since the bigger gaps in temperature could cause severe bottlenecks in communication across the temperature ladder.

When N is large, the differences in acceptance ratios between a geometric ladder and one chosen for uniform A becomes less significant. In this case, the difference between the limiting (minimum) acceptance ratio for a ladder and the ladder’s average acceptance ratio is proportionally smaller.

In the case of the double Rosenbrock distribution (20), we have found that, once the minimum acceptance ratio for a geometric ladder (terminating at $T_{\text{max}} = 2 \times 10^4$) exceeds $\sim 10\%$, reallocating temperatures for uniform acceptance ratios does not reduce the measured ACT by more than 25%. This occurs when $N \approx 7$ in the current example. Nonetheless, there remains an overall improvement in ACT regardless of N .

Figure 10 also shows, in the middle pane, the total number of iterations per independent sample across all chains. This quantity, given by $N \times \tau$, is proportional to the total CPU time of the simulation, while τ itself is proportional to the CPU time per chain, or *wall time*, of the simulation. In this instance, the CPU time of a run diminishes with N in much the same fashion as the wall time does. The fractional improvement in CPU time is of course the same as for wall time – $\tau_{\text{geo}}/\tau_{\text{acc}}$.

4.2.3 Test: chain removal

To determine whether a uniform- A temperature placement strategy is in fact close to optimal, we assess the contribution of each chain from such a temperature ladder to the efficiency of the sampler, as measured by its ACT. If this contribution is equal for all chains, then we can conclude that it is indeed optimal to have them all exchanging equally – that is, with uniform acceptance ratios.

To this end, we conducted the following test:

(i) Sample from (20) with $N = 7$ chains under the temperature dynamics of Section 3 until the temperatures have equilibrated to (T_1, \dots, T_7) to give uniform acceptance ratios.

(ii) Generate 5 new test ladders, each of 6 chains, formed by removing the i^{th} chain from that determined above – i.e., $(T_1, \dots, T_{i-1}, T_{i+1}, \dots, T_7)$ – for $i = 2, \dots, 6$.

(iii) Sample from (20) with each of these 5 test ladders and calculate the ACTs on the cold chain, τ_{test} .

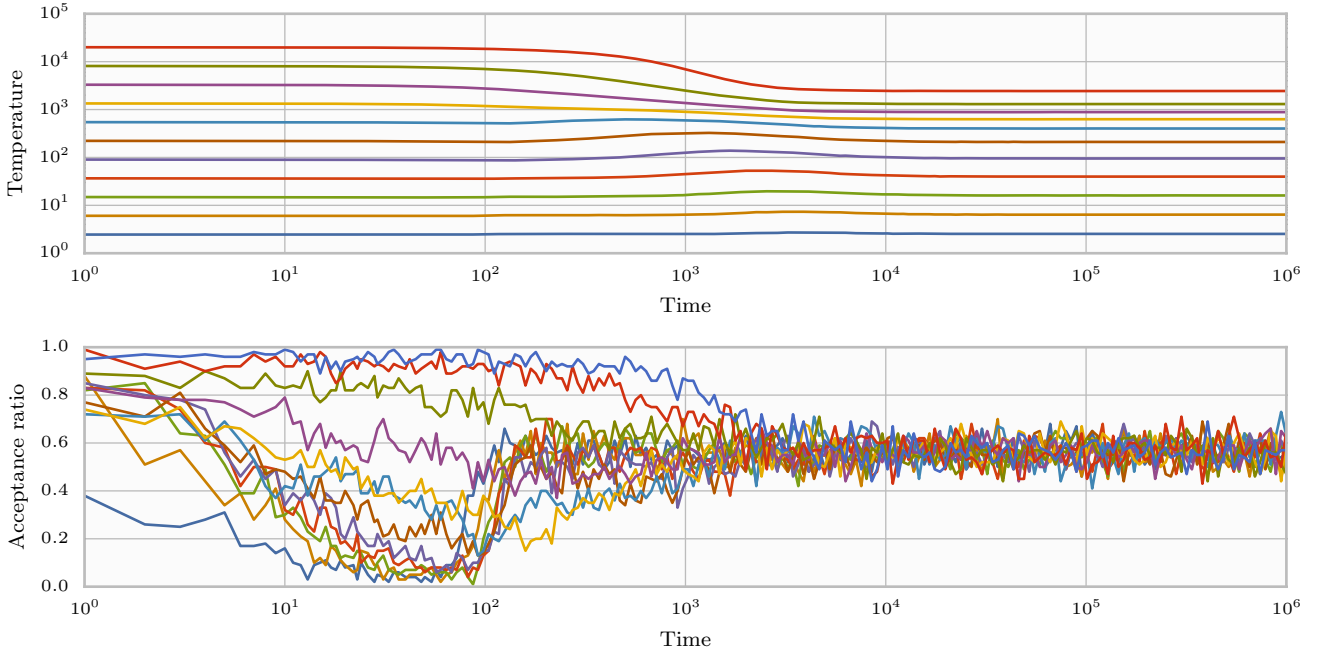


Figure 8. The evolution of ladder of 13 temperatures T_i and acceptance ratios A_i over an EMCEE run of 10^6 iterations under the Rosenbrock likelihood (20). Chains 1 and 13 are not shown, having fixed temperatures $T_1 = 1$ and $T_{13} = \infty$.

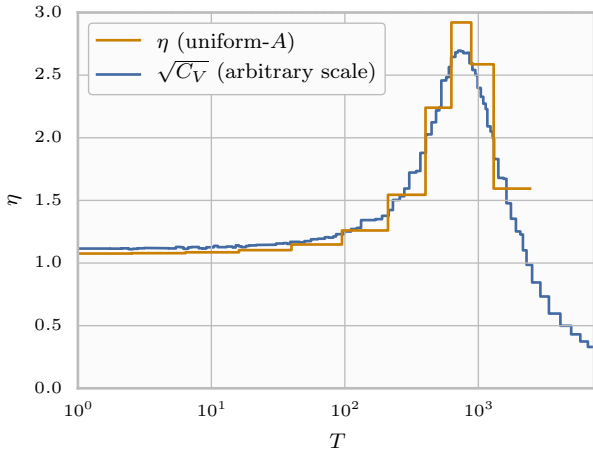


Figure 9. **Orange:** The equilibrium density of chains per log T for the double Rosenbrock run illustrated in Figure 8, where the acceptance ratios have settled to $A_i \approx 0.57$. **Blue:** The square root of the specific heat for the double Rosenbrock distribution, as described in Figure 6.

Figure 11 shows the ACTs for the cold chain resulting from the test outlined above. While $\tau_{\text{acc}} < \tau_{\text{test}} < \tau_{\text{geo}}$ for ladders of the same N , τ_{test} increases with the temperature of the chain that is removed, suggesting that additional chains are more useful at higher temperatures. The sharp jump in τ_{test} when a chain above $T \approx 200$ is removed arises from the phase transition that occurs as T approaches T_{prior} , indicated by a peak in C_V (visible in Figure 9).

We can understand this behaviour by examining the complete autocorrelation functions from which these ACTs are estimated. Illustrated in Figure 12, these autocorrelation functions exhibit two distinct time-scales. Firstly, there is a large autocorrelation for lags $\lesssim 100$ for all i – particularly $i = 2$ – corresponding to the ACT of the sampler within one of the two modes: that is, the time taken for the sampler to generate an independent sample without changing mode. Secondly, there is a visible hump in the autocorrelation function for $100 \lesssim \text{lag} \lesssim 2000$, corresponding to the time taken for the sampler to migrate between modes. Removing the second chain from initial geometric ladder of 7 chains increases the intra-mode ACT in particular, but does not affect the inter-mode ACT. Meanwhile, while removing higher temperature chains pushes the secondary hump outward to larger lags, increasing the inter-mode ACT instead.

The overall autocorrelation time in which we are interested, discussed by Sokal (1997) and in Appendix A, represents the time between independent samples of the system. It is therefore set by the time-scale on which the sampler migrates to a new mode independently of the current mode. Removing a chain at higher temperatures increases the inter-modal ACT, and therefore damages the efficiency of the sampler.

Nonetheless, all of the tested temperature ladders yielded lower ACT than the default geometric ladder, despite the geometric ladder being chosen with prior knowledge of T_{prior} .

4.3 Egg-box in five dimensions

To test the algorithm’s performance on a yet more strongly multi-modal distribution, we use an egg-box distribution de-

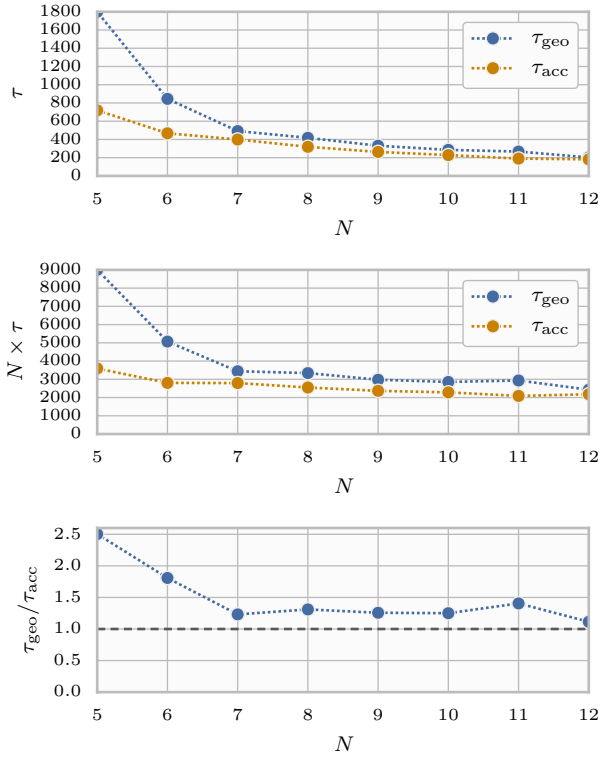


Figure 10. **Top:** the ACTs of x for the cold ($T = 1$) chain of a sampler exploring the double Rosenbrock distribution (20), using both uniform- A and geometrically spaced temperature ladders as a function of the number of chains N . **Middle:** the total CPU time, $N \times \tau$, for the runs. **Bottom:** the relative improvement in the ACT for the uniform- A ladder over the geometric ladder. The joining lines are provided to guide the eye.

finied by the likelihood

$$L(\vec{\theta}) \propto \left(\frac{1}{2} \prod_{i=1}^n \cos \theta_i + \frac{1}{2} \right)^{1/T_p}. \quad (22)$$

For a small value of the pre-tempering factor T_p the modes of this distribution become locally Gaussian, and in the low- T regime should therefore generate results similar to those of the Gaussian distributions examined in Section 2.2 and Section 4.1. For the following tests, we choose $T_p = 10^{-3}$.

We explore this likelihood distribution in 5 dimensions over a flat prior on $[-L/2, L/2]^n$, where we choose $L = 3\pi$, giving $3^n = 243$ modes.

Rather than compare our uniform- A temperature ladder against a geometric ladder with a fixed maximum temperature, as in Section 4.2, we instead use a geometric ladder constructed to give a fixed acceptance ratio of $E[A] = 0.25$ when applied to the special case of an ideal Gaussian likelihood (per Section 2.2). Such a ladder will not, in general, give uniform acceptance ratios when applied to an arbitrary posterior distribution, but this choice reflects the more realistic scenario where we cannot guess at T_{prior} , and so we resort to assuming that the distribution indeed behaves like an ideal Gaussian.

Figure 13 shows the evolution of the temperatures and

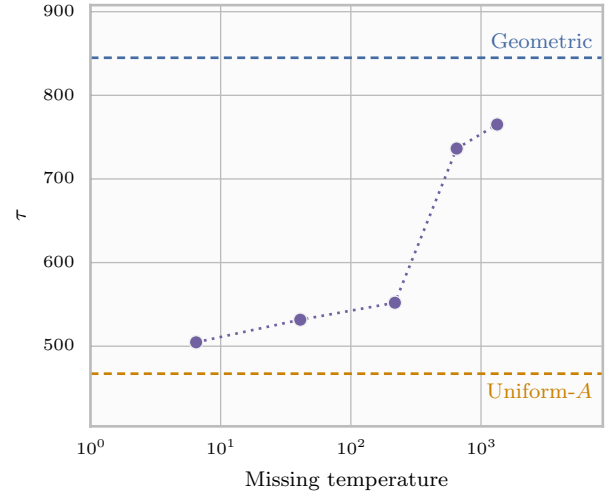


Figure 11. The cold-chain ACTs for samplers exploring the double Rosenbrock distribution (20) per the test described in Section 4.2.3. The points denote the ACTs from ladders generated according to the scheme in Section 4.2.3. The dashed lines above and below identify the ACTs from geometric and uniform- A ladders, respectively, of $N = 6$.

acceptance ratios for an EMCEE sampler of 15 chains under the temperature dynamics of Section 3. Figure 14 shows the equilibrium density $\eta(\log T)$ after the ladder has achieved uniform acceptance ratios.

Figure 15 shows the ACTs of the cold chain ($T = 1$) under uniform- A and geometric ladders for the 5-dimensional egg-box problem as a function of the number of temperatures available. In this case, adding more temperatures to a geometric ladder does not reduce the measured ACT of the sampler for $N \geq 7$, since they are added to the high- T end of the ladder, above T_{prior} , and the ratios between lower temperatures do not change. Figure 13 shows that from the initial geometric ladder only around 6 chains are within the range of temperatures spanned by the equilibrium ladder; the remaining 8 (excluding $T_1 = 1$ and $T_N = \infty$) are all above T_{prior} and effectively sample from the prior. In this case, therefore, the geometric spacing that would give uniform acceptance ratios of 25% for an ideal Gaussian in fact spaces temperatures too widely for $\gtrsim 6$ chains.

Meanwhile, adding more chains to a dynamically adapted ladder clearly reduces the ACT of the sampler in this regime. Moreover, the ACT of a sampler using a uniform- A ladder is always lower than that of a sampler using the geometric ladder of the same N . In the egg-box example, which requires a relatively close spacing of temperatures, the improvement is dramatic when many chains are used: $\tau_{\text{geo}} > 2\tau_{\text{acc}}$ for $N \geq 12$.

The failure of the geometric ladders used in this example for $N \geq 7$ lies in the poor T_{max} chosen by assuming that the distribution behaves like an ideal Gaussian. A geometric spacing is in fact appropriate for a large portion of the temperature range, but its efficacy relies on the ladder terminating at the correct T_{prior} .

When $N < 7$, the geometric and uniform- A ladders show similar ACTs, and the geometric ladders in fact do

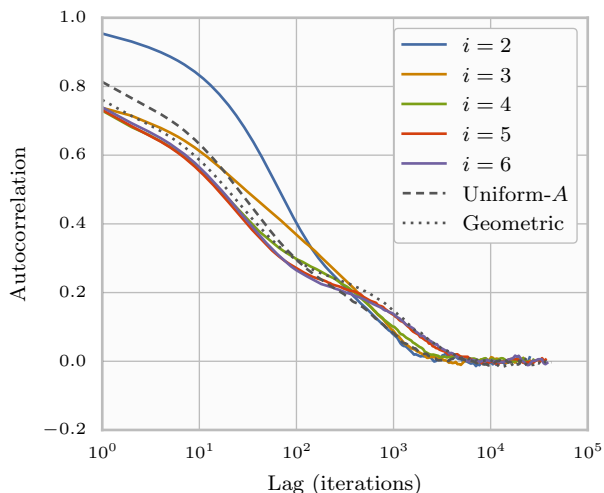


Figure 12. The cold-chain autocorrelation function for a sampler exploring the double Rosenbrock distribution (20). The solid lines correspond to the ladders generated by the scheme outlined in Section 4.2.3, where i is the index of the removed chain. For comparison, the dashed and dotted lines represent respectively uniform- A and geometric ladders of the same size. The approximate ACTs are 504, 531, 551, 736, and 765, for $i = 2, \dots, 6$; 467 for a uniform- A ladder; and 844 for a geometric ladder (see Figure 11).

slightly *better*. While unexpected, this is a consequence of the behaviour of the affine invariant ensemble sampler used in EMCEE (Foreman-Mackey et al. 2013; Goodman & Weare 2010) as applied to the egg-box likelihood (22). When such a sampler is applied to a target distribution for which the number of modes n_m is greater than the number of walkers n_w used by the sampler, it behaves as though it is sampling from the prior (albeit inefficiently). There is therefore little benefit in having a chain sampling as high as T_{prior} , and so it is better – in terms of the ACT – to assign more chains to lower temperatures in order to increase their acceptance ratios. In our case, the egg-box likelihood has 243 modes in 5 dimensions, while the sampler uses only 100 walkers, so these walkers tend to become isolated from one another. Since the sampler relies on clustering of walkers on an individual mode to inform jump proposals within that mode, jumps are instead proposed *between* modes when there are on average fewer than one walker per mode.

We anticipate that running the same tests on a traditional single-walker MCMC sampler, or reducing the number of modes of the likelihood distribution so that $n_w \gg n_m$, will dramatically increase $\tau_{\text{geo}}/\tau_{\text{acc}}$ in the low temperature regime. We should expect that $\tau_{\text{geo}} \gg \tau_{\text{acc}}$ when $T_{\text{max}}(N) \ll T_{\text{prior}}$ for the geometric ladder and that $\tau_{\text{geo}} \approx \tau_{\text{acc}}$ when $T_{\text{max}}(N) \approx T_{\text{prior}}$.

Figure 15 therefore illustrates a very specific case for $N < 7$ that does not reflect the importance of choosing $T_{\text{max}} \approx T_{\text{prior}}$. Nonetheless, the ACTs of the two temperature allocation strategies – geometric and uniform- A – are still fairly similar for $N \leq 7$ and there is a distinct improvement for $N > 7$.

5 GRAVITATIONAL WAVE SIGNALS FROM COMPACT BINARY COALESCENCES

We now present an example application of the dynamics of Section 3 to a challenging and computationally expensive astrophysical inference problem.

The first direct detections of gravitational waves (GWs) by ground-based GW detectors comprising the advanced LIGO and Virgo observatories (Aasi et al. 2015; Acernese et al. 2015) are anticipated within this decade. Among the most promising candidate sources for these detectors are extragalactic compact binary coalescences (CBCs) (Abadie et al. 2010): the energetic inspiral and merger of pairs of neutron stars and/or black holes, emitting a well-modelled GW signal.

For GW astrophysicists, recovery of the source parameters of such a signal from the GW signature as observed by the detectors is a significant challenge in the application of Bayesian statistics (e.g., van der Sluys et al. 2008a,b; Raymond et al. 2010; Rodriguez et al. 2014; Aasi et al. 2013; Vitale et al. 2014; Singer et al. 2014; Veitch et al. 2015). Parallel-tempered MCMC is one method used within the LIGO Scientific Collaboration (LSC) to perform this inference, so parameter estimation for CBC detections presents an ideal test for the scheme outlined in Section 3.

5.1 Parameter estimation for gravitational waves

We aim to recover the Bayesian posterior probability density $\pi(\vec{\theta})$ for the parameters $\vec{\theta}$ of a merging binary system from which a GW signal has been detected, given some detector data s and priors $p(\vec{\theta})$.

The likelihood function $L(\vec{\theta}; s)$ for this problem is a function of

- (i) the detector output s , and
- (ii) a model waveform $h(\vec{\theta})$ representing a putative GW signal,

such that $s = h(\vec{\theta}) + n$, where n is the noise in the detector and s , h , and n are time series with Fourier transforms \tilde{s} , \tilde{h} , and \tilde{n} respectively.

Given a noise model for the detector, \tilde{n} is then a random variable with a known distribution and $L(\vec{\theta}; s)$ can be defined in terms of $\tilde{n} = \tilde{s} - \tilde{h}(\vec{\theta})$. Under a simple stationary Gaussian noise model this likelihood can be expressed as

$$\log L(\vec{\theta}; s) = -\frac{1}{2} \int_{-\infty}^{\infty} \frac{|\tilde{s}(f) - \tilde{h}(f; \vec{\theta})|^2}{S_n(f)} df + C, \quad (23)$$

where C is a normalising constant and S_n is the two-sided noise power spectral density (PSD).

The approximate CBC waveform h that determines this likelihood has between 9 and 15 physical parameters in $\vec{\theta}$. These parameters can be partitioned into two disjoint groups; firstly, the intrinsic parameters are those that determine the dynamics of the source itself:

- q and \mathcal{M} : the mass ratio and chirp mass of the binary, system⁷,

⁷ This is an alternative parameterisation of the mass configuration of a binary system with component masses m_1 and m_2 , such that $q \equiv m_2/m_1$ and $\mathcal{M} \equiv (m_1 m_2)^{3/5}/(m_1 + m_2)^{1/5}$.

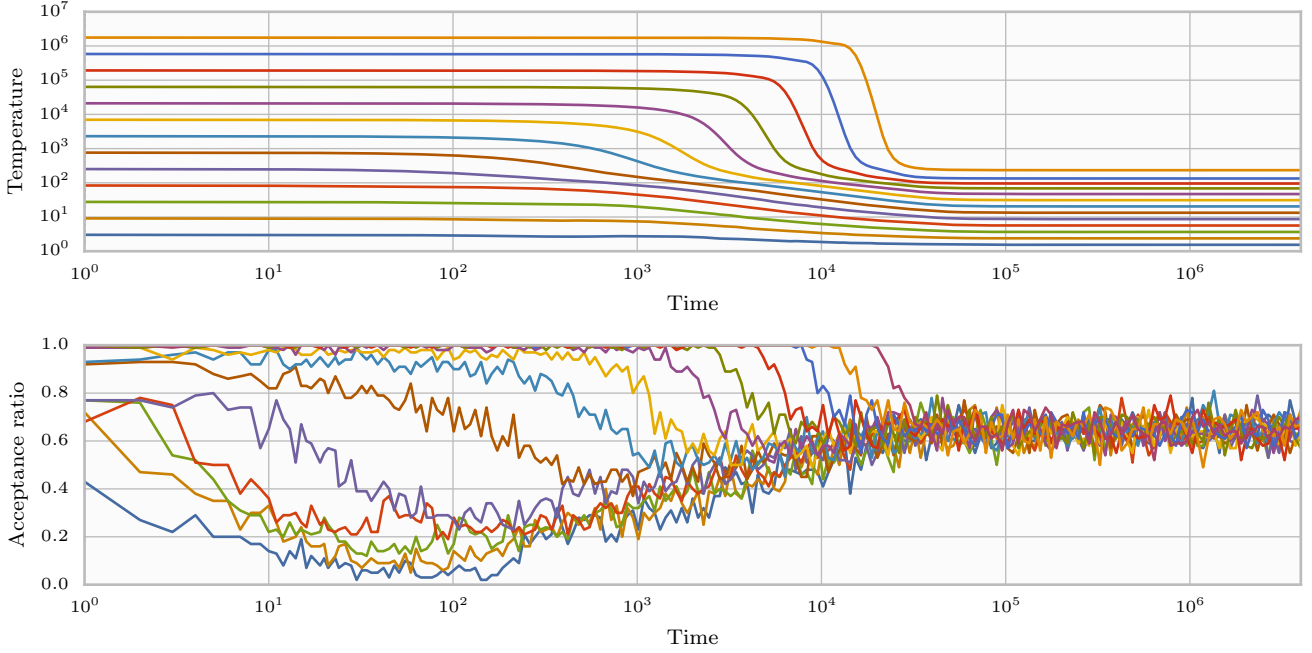


Figure 13. The evolution of temperatures T_i and acceptance ratios A_i while sampling with EMCEE from a 5-dimensional egg-box distribution, (22), with 15 chains. Chains 1 and 15 are not shown, having fixed temperatures $T_1 = 1$ and $T_{15} = \infty$.

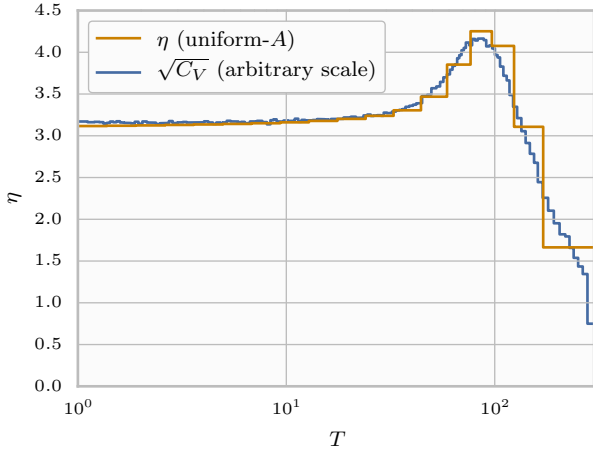


Figure 14. **Orange:** The equilibrium density of chains per $\log T$ for the egg-box run illustrated in Figure 13, where the acceptance ratios have settled to $A_i \approx 0.65$. **Blue:** The square root of the specific heat for the egg-box distribution, as described in Figure 6.

- a_1 and a_2 : the spin magnitudes of the binary components, and
- t_1, t_2, ϕ_{JL} , and ϕ_{12} : the four angles describing the spin orientations of the binary components.

Secondly, the extrinsic parameters are those that determine only the waveform observed at the detector:

- d_L : the luminosity distance between the binary system and the detector,

- α and δ : the right ascension and declination of the event,
- ψ and θ_{JN} : the two angles describing the orbital orientation of the binary system, and
- t_c and ϕ_c : a reference time and phase for the waveform.

A binary system with arbitrary spinning component masses is therefore described by 15 parameters. A binary system whose spins are aligned with its orbital axis is modelled by 11 parameters, neglecting the spin orientation angles, and a non-spinning system is modelled by only 9 parameters, with the spin magnitudes also omitted.

This likelihood function and its parameter space generate a highly structured posterior distribution with many modes and degeneracies that is difficult for conventional MCMC samplers to explore.

5.2 Dynamic parallel tempering

We implemented the scheme of Section 3 in the MCMC sampler used by LALINFERENCE: the software suite used by the LSC for GW parameter estimation (Veitch et al. 2015). Unlike EMCEE, the LALINFERENCE sampler uses only one walker, with jump proposals that are tuned to the structure of the posterior distribution generated by a CBC signal. Veitch et al. (2015) present a comparison of LALINFERENCE’s standard parallel tempered MCMC implementation with other sampling techniques, such as nested sampling (Skilling 2006; Veitch & Vecchio 2010). They find MCMC to be at least competitive with the other methods in both CPU time and wall time, and in some cases better.

To compare our implementation of Section 3 under LALINFERENCE with the default geometric temperature ladder, we tested both schemes on a number of synthetic

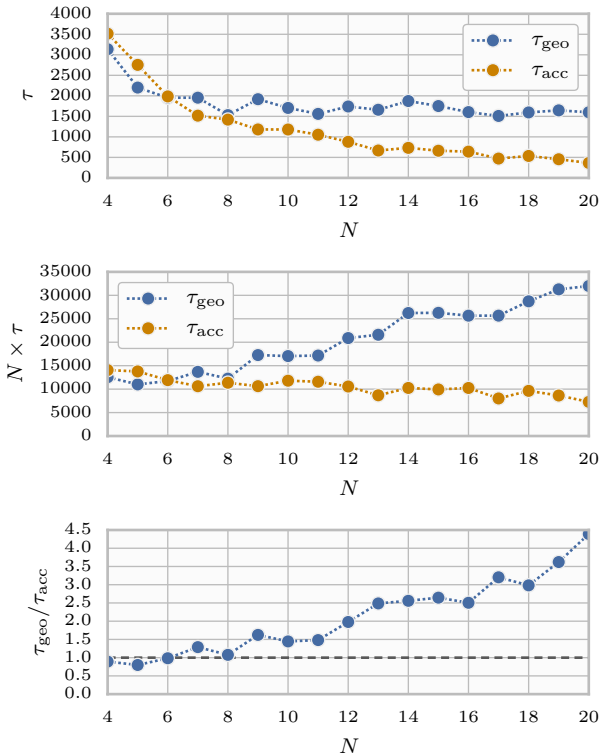


Figure 15. **Top:** the ACTs of the cold chain ($T = 1$) of a sampler exploring the egg-box likelihood (22) with ladders of different sizes N , for both geometric temperature ladders and ladders dynamically adapted for uniform acceptance ratios. **Middle:** the total CPU time, $N \times \tau$, for the runs. **Bottom:** the relative improvement in ACT conferred by dynamically adapting for uniform acceptance ratios over a geometric ladder.

GW events simulating the signals received from two different compact binary sources.

We conduct our tests against two non-spinning prototype GW sources: a binary neutron star (BNS) system and a binary black hole (BBH) system, detailed in Table 1. For each of these prototypes, we simulate coherent detections by a network of GW detectors, for a range of network signal-to-noise ratios (SNRs), by injecting the computed GW signal into mock Gaussian noise generated from the noise PSDs of each detector. We simulate a network comprising the Advanced LIGO detectors in Hanford, Washington and Livingston, Louisiana and the Advanced Virgo detector in Cascina, Italy, using noise PSDs that approximate the detectors’ design sensitivities (The LIGO Scientific Collaboration 2010; The Virgo Collaboration 2009).

The SNR ρ of a GW detection is a proxy for the maximum log likelihood, such that $\Delta \log L$ scales as $\rho^2/2$, where $\Delta \log L$ is the difference between the maximum log likelihood under the signal model and the likelihood of the noise-only ($h = 0$) model. The SNR therefore indicates how sharply peaked the posterior distribution will be. Since the SNR of a detection can be estimated by the detection pipeline, it can also be used to decide the T_{max} used in constructing a geometric temperature ladder for that run, against which we compare a uniform- A ladder.

We attempt to recover the parameters of the injected events with the likelihood function (23), using two families of frequency-domain waveform approximants:

(i) *TaylorF2*, which describes with 9 to 11 free parameters the post-Newtonian inspiral of two masses, optionally with spins aligned with the orbital axis (Buonanno et al. 2009), and

(ii) *IMRPhenomP*, which describes the full inspiral-merger-ringdown sequence of a CBC, allowing for arbitrary precessing spins and having 15 free parameters (in the LALINFERENCE implementation) (Hannam et al. 2014).

When recovering with *TaylorF2*, we allow for aligned spins in the system, while for both approximants, we analytically marginalise the reference phase ϕ_c out of the likelihood. For our runs, therefore, the *TaylorF2* approximant generates a 10-dimensional parameter space, while *IMRPhenomP* generates a 14-dimensional parameter space.

The posterior distribution for one of these problems, a BNS binary recovered with *TaylorF2* at an SNR of 25, is illustrated in Figure 16 and Figure 17. These show the one- and two-dimensional marginal distributions of the recovered samples, partitioned into intrinsic and extrinsic parameters. Some parameters, such as the chirp mass \mathcal{M} , are very accurately measured, while others show multiple modes (e.g., the polarisation angle ψ) or strong correlations (e.g., distance d_L and inclination θ_{JN}).

Figure 18 shows the effect of the SNR on the equilibrium (uniform- A) chain density η selected by our dynamical scheme. While the structure of the temperature ladder is preserved, its features scale to higher temperatures as the SNR of the injected signal increases while the average value of η falls. Since the maximum log likelihood scales with the square of the SNR, it follows that, under a fixed prior, T_{prior} should also increase with the SNR.

Meanwhile, Figure 19 shows the ratios of ACTs for runs using uniform- A ladders versus those using geometric ladders. The lowest SNR that we simulate, 10, represents a signal that is on the threshold of detectability, where we expect most detections to occur, while the maximum, 25, represents a relatively loud signal (at around the 90th percentile of detectable events).

While there is significant variation in the ACT measurements between SNRs, there is on average a reduction in ACT of 26% for the systems and SNRs tested. In general, a uniform- A ladder is at least as effective as a geometric ladder in all cases; that is, the ACT ratio $\tau_{\text{geo}}/\tau_{\text{acc}}$ is never less than one (within error bars). In some cases, this ratio is appreciably greater than one, e.g., for low-SNR BNS events.

However, as we shall discuss briefly in Section 6.1, the single-walker nature of the LALINFERENCE sampler inhibits communication between the extremal chains, so that the temperatures are in fact partitioned into two independent, non-communicating groups. The improvement we observe in Figure 19 therefore arises in fact from more efficient allocation of the temperatures below the critical temperature of the phase transition. Meanwhile, those chains above the critical temperature – which are sampling in the regime where the noise-only model is preferred over the presence of a GW signal – remain isolated.

We anticipate that, with an ensemble sampler with similar problem-specific optimisations to those used by

LALINFERENCE, the communication barrier at the phase transition could be removed and we may observe greater improvements in ACT and sampling efficiency.

6 DISCUSSION

The temperature selection scheme set out in Section 3 solves two problems in the application of parallel tempering:

(i) It identifies $T_{\max} = \infty$ as a suitable temperature for the hot chain – such that it will sample from the prior – that is independent of the target distribution.

(ii) It allocates a fixed number of intermediate temperatures to ensure good communication between fixed extremal temperatures T_{\min} and T_{\max} , and therefore efficient sampling of the target distribution – i.e., with few iterations between independent samples.

The intermediate temperatures are allocated so that acceptance ratios for swaps proposed between neighbouring pairs of chains are uniform across the temperature ladder. The dynamical algorithm that implements this scheme requires only two parameters: ν and t_0 . These parameters, discussed in Section 3.2, describe only the initial dynamics of the temperatures, setting the time-scale for temperature adjustments, and do not determine the equilibrium uniform- A ladder.

While a temperature configuration that is selected for uniform acceptance ratios between all chain pairs is not necessarily *optimal* in the ACT of the sampler, we have demonstrated that it is generally better than a conventional geometric temperature configuration and provides more consistent behaviour across different likelihood distributions and numbers of chains. Importantly, the dynamics that achieve such a temperature ladder are simple and easily implemented, requiring very little tuning or intervention.

The factor by which the ACT is reduced by the uniform- A scheme depends strongly on the likelihood distribution that is explored and on the specific geometric ladder against which the uniform- A scheme is being compared. For a geometric ladder, one must make an ad hoc choice of the maximum temperature T_{\max} ; this is difficult and a poor guess can yield a very sub-optimal ladder. In particular, if T_{\max} is not high enough that the sampler can efficiently migrate between modes, then the ACT will be significantly higher than it needs to be. On the other hand, if T_{\max} is too high, then many of the chains will effectively sample from the prior, and CPU time will be wasted in sampling from redundant tempered likelihood distributions.

The uniform- A temperature dynamics guarantee that, for a given number of chains N , no such wastage of CPU time occurs and that there will always be precisely one chain sampling at $T_{\max} = \infty$ (i.e., sampling from the prior). Tests of the dynamics generally demonstrate lower ACTs when compared with geometric temperature ladders of the same number of chains, N .

In Section 4.2.2 we demonstrated that, even with a judicious choice of T_{\max} that is close to T_{prior} , a traditional geometric ladder is outperformed by a ladder chosen for uniform acceptance ratios (with $T_{\max} = \infty$). Figure 10 illustrates that, when T_{prior} is known, a uniform- A ladder confers the greatest reduction in ACT when N is small. In

this case, the temperature ratio γ of the geometric ladder is large enough that phase transitions in the distribution of $\log L$ cause a bottleneck in the communication between hot and cold chains around a critical temperature, where $A \ll 1$. The uniform acceptance scheme allocates more chains over these temperature regimes in an effort to optimise the communication.

For larger N , $\tau_{\text{geo}}/\tau_{\text{acc}} \approx 1$, suggesting that – as long as there are no pairs of chains with prohibitively low swap acceptance ratios – a geometric spacing is adequate if T_{\max} is chosen appropriately.

It is unclear how to determine the threshold A below which communication is impeded, but it is likely related to the time-scale of the intra-chain motion of the sampler. If intra-chain jumps are accepted seldom with respect to the rate of inter-chain swaps, then increasing the inter-chain swap acceptance ratio is unlikely to make the sampler any more efficient.

In general, while $\tau_{\text{geo}} > \tau_{\text{acc}}$ for all N , the improvement fraction $\tau_{\text{geo}}/\tau_{\text{acc}}$ will asymptote to 1 as $N \rightarrow \infty$. The rate of decay will depend strongly on the target distribution. A system with a wide distribution of $\log L$ (e.g., with many dimensions) or with sharp phase transitions at certain temperatures (e.g., with many modes of various shapes and weights) will see the most benefit from having many chains, while a better-behaved distribution without such features can be efficiently sampled with fewer.

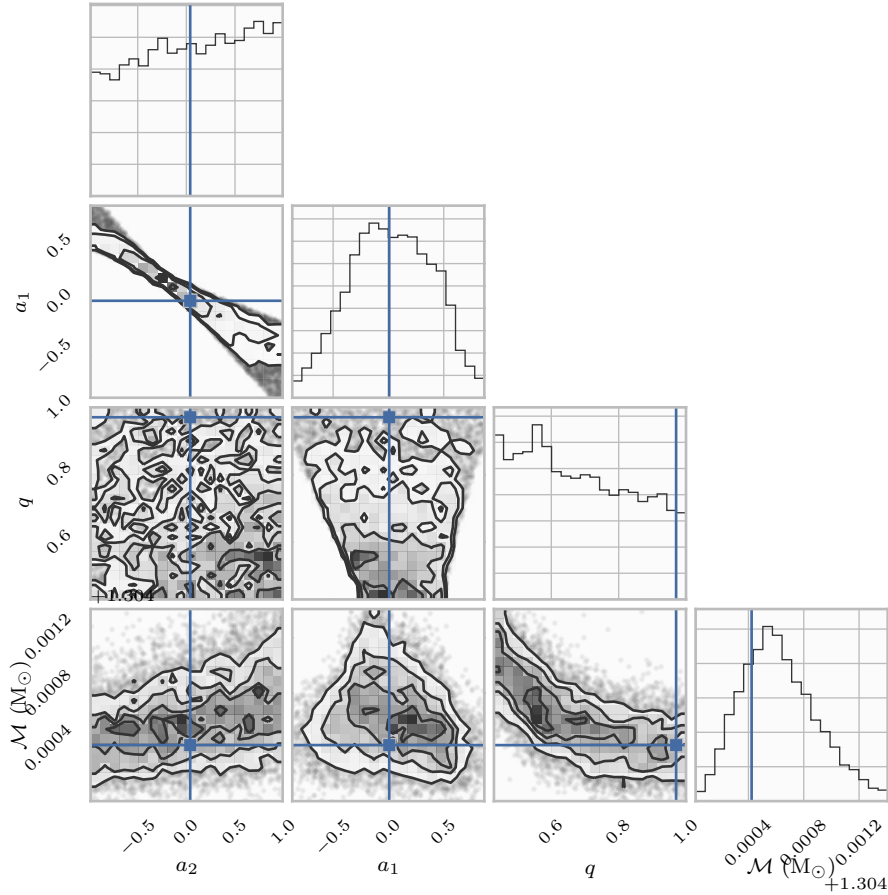
Meanwhile, from our tests on the 5-dimensional egg-box distribution discussed in Section 4.3, we can see the consequences of a poor choice of T_{\max} . While the egg-box distribution does not have as strong a phase transition as the double Rosenbrock function of Section 4.2, our ignorance of T_{prior} means that a geometric ladder (which in this case is constructed from a fixed temperature ratio γ) is mostly worse than a uniform- A ladder. Figure 15 demonstrates this, specifically when N is large enough that for a given γ the geometric ladder places many temperatures redundantly above T_{prior} . In this case, we see a dramatic improvement in ACT τ from using a uniform- A ladder when compared with a geometric ladder of the same number of chains N ; indeed, the ratio $\tau_{\text{geo}}/\tau_{\text{acc}}$ becomes as large as ~ 4 for the values of N tested. Since τ_{geo} is independent of N when $N \gtrsim 7$, we should expect that this ratio will saturate as $N \rightarrow \infty$, where τ_{acc} reaches a minimum. Moreover, the CPU time, $N \times \tau$ of the uniform- A runs continues to decrease with N in the explored range, even as the CPU time of the geometric runs rises.

On the other hand, when N is too small for a geometric ladder to reach the prior (i.e., $T_N \ll T_{\text{prior}}$), we notice that in fact $\tau_{\text{geo}} < \tau_{\text{acc}}$. As discussed in Section 4.3, this somewhat surprising result arises from a limitation of the ensemble sampler that was used to sample the distribution. We anticipate that if the number of walkers were increased to many times the number of modes – which is required for efficient sampling – the geometric ladder will fail dramatically in this regime of N , giving $\tau_{\text{geo}} \gg \tau_{\text{acc}}$.

Finally, our astrophysical application in Section 5 illustrates the use of the scheme of Section 3 in a single-walker setting. In this case, a uniform- A ladder improves on the default geometric ladder used by LALINFERENCE, giving on average a 26% reduction in ACT. These tests do, how-

Table 1. The CBC event prototypes used to test the adaptation scheme of Section 3. All prototypes are simulated at distances that yield 5 different SNRs: 10, 11, 15, 19, and 25.

Source	Injection waveform	q	$\mathcal{M} (M_{\odot})$	Recovery waveforms
BNS	<i>SpinTaylorT4</i>	0.970	1.30	<i>TaylorF2</i>
BBH	<i>IMRPhenomP</i>	0.996	4.82	<i>TaylorF2, IMRPhenomP</i>

**Figure 16.** The one- and two-dimensional marginal distributions of the intrinsic parameters of a BNS event with SNR 25. Note, in particular, the very accurate measurement of the chirp mass \mathcal{M} (the plotted range is only $\sim 0.1\%$ of the true value).

ever, reveal an instability in the uniform- A dynamics under a single-walker sampler, which we describe below.

6.1 Single-walker implementation

The dynamical algorithm set out in Section 3 can be implemented in a traditional MCMC sampler that uses only a single sample per chain, with reductions observed in the ACT of the sampler relative to a geometric temperature ladder, as shown in Section 5.2. However, in this case, equal (and large) acceptance rates between all chains do not guarantee good communication of sample positions between extremal temperatures.

A complex, multidimensional posterior such as that described in Section 5.2 may exhibit a phase transition. At $T = 1$, the posterior is dominated by the likelihood peaked around the true parameter values; at $T = \infty$, it is domi-

nated by the much larger prior volume far away from the parameter values, corresponding to a weak or absent signal; and at the phase transition temperature, the two contribute comparably to the posterior, which is distinguished by two distinct likelihood peaks: a high-likelihood peak near the signal parameters, and a low-likelihood peak in the region of significant prior support. In effect, this becomes a reversible-jump MCMC problem with two distinct modes: the high-likelihood signal model, and the low-likelihood noise-only model.

The dynamical algorithm with a single walker has a tendency to select very small temperature gaps around phase transitions. From (2), when $\Delta\beta \rightarrow 0$, $A \rightarrow 1$ regardless of the likelihoods of the chains. However, the likelihood distributions near the phase transition temperature will be distinct enough that there is no intra-chain migration of samples between them. Consequently, despite efficient communica-

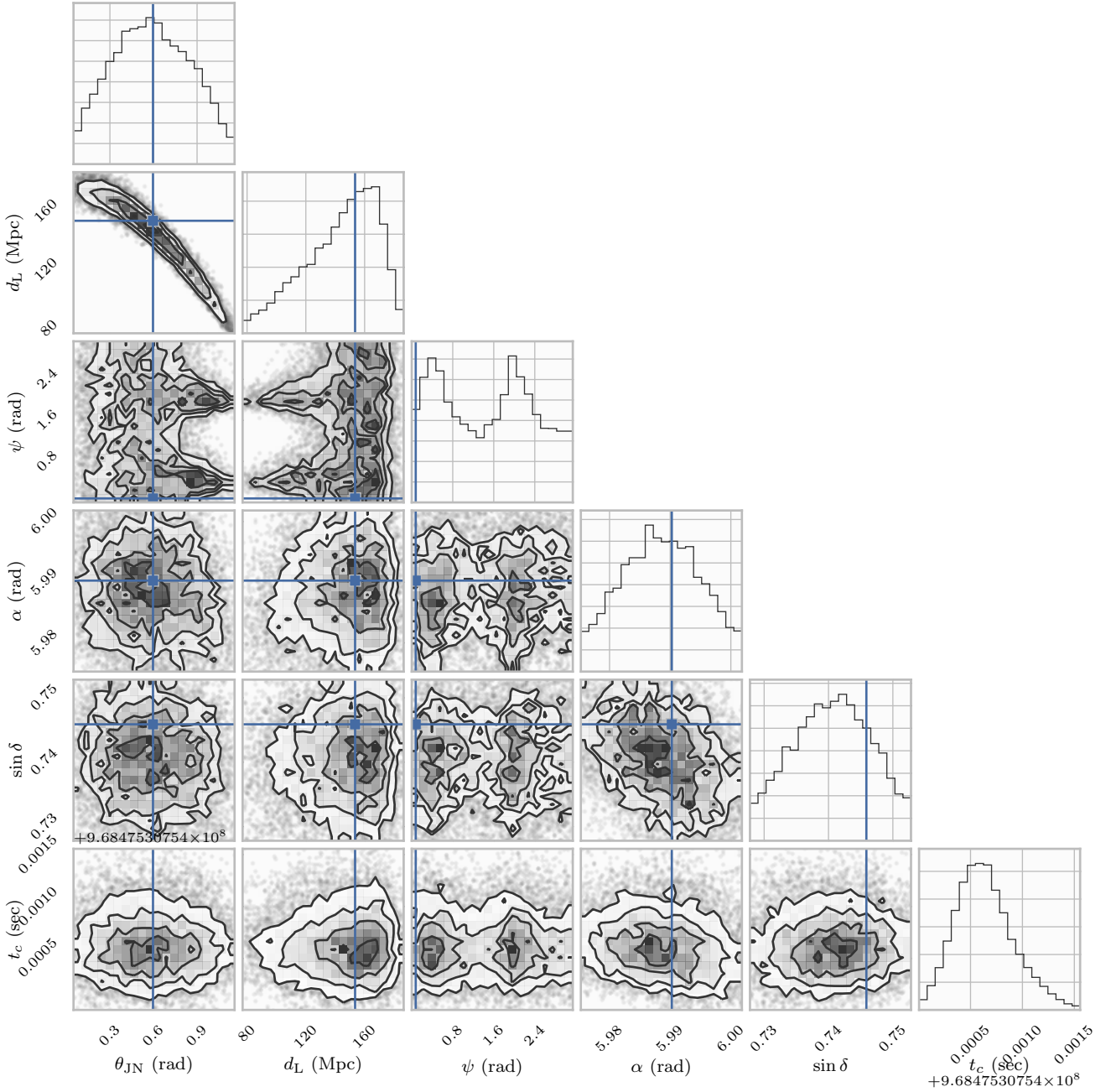


Figure 17. The one- and two-dimensional marginal distributions of the extrinsic parameters recovered with *TaylorF2* from a BNS event with SNR 25. Note the multiple modes for the polarization angle ψ and the strong correlation between distance d_L and inclination θ_{JN} .

tion between chains, the higher temperatures do not help low-temperature walkers to efficiently jump between the two modes, since the high- and low-likelihood modes do not mix well at any temperature.

Figure 20 demonstrates how large acceptance ratios do not guarantee the transmission of sample positions between low and high temperatures when there is only one sample per temperature. In this case, 9 samples (whose paths are shown as dotted lines) occupy the high- $\log L$ part of the parameter space representing the signal model, while the remaining 3 (solid lines) occupy the low- $\log L$ part, representing the

noise-only model. This barrier occurs at the temperature at which the evidence for the noise-only model is equal to that of the signal model.

We did not encounter this issue with an ensemble sampler, which is less susceptible to this instability because it allows the ensemble at each temperature to occupy both models simultaneously.

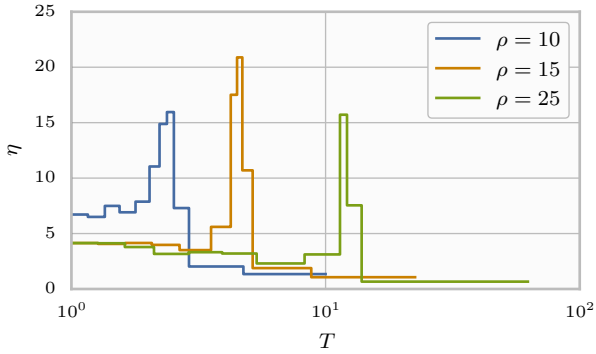


Figure 18. The equilibrium density of chains per $\log T$, from (19), for the *TaylorF2* BBH runs described in Section 5.2 at various SNRs.

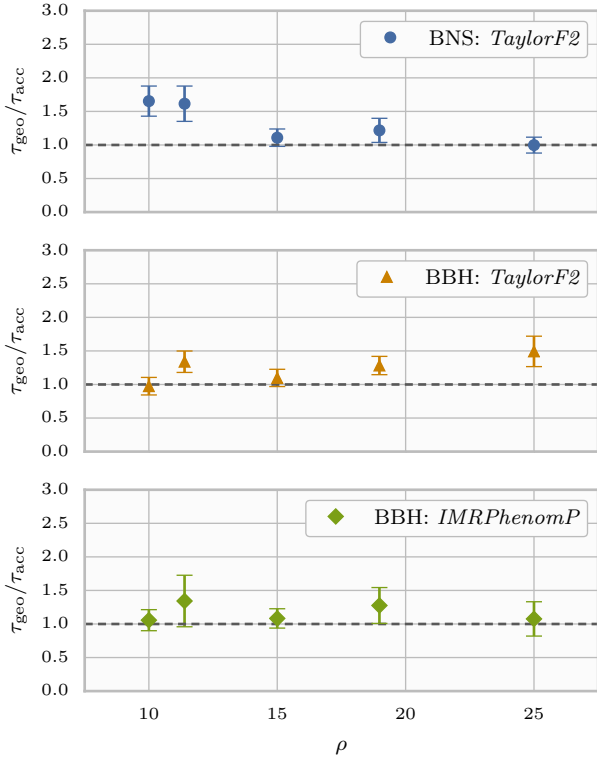


Figure 19. The fractional improvements in ACT conferred by a uniform- A temperature ladder over a geometric ladder for the CBC parameter estimation problem described in Section 5.2 at various SNRs.

6.2 Evidence calculations

The current paper focuses mainly on the efficiency of a parallel tempered MCMC sampler in producing independent samples from its target distribution. Another important task in Bayesian statistical inference is to compute the evidence integral of the posterior distribution. At a given tempera-

ture, this is given by

$$Z(\beta) \equiv \int L(\vec{\theta})^\beta p(\vec{\theta}) d\vec{\theta}, \quad (24)$$

where $\beta \equiv 1/T$ is the inverse temperature.

Since we are interested in the untempered posterior, we wish to calculate $Z(1)$. From (24), we can use thermodynamic integration (Goggans & Chi 2004; Lartillot & Philippe 2006) to express the log evidence (relative to the prior) in terms of the mean $\log L$, such that

$$\Delta \log Z \equiv \log Z(1) - \log Z(0) = \int_0^1 \mathbb{E}[\log L]_\beta d\beta, \quad (25)$$

to which the logarithm of the integral of the prior, $\log Z(0)$, can be added to give the absolute evidence $\log Z(1)$.

The log evidence can therefore be computed by a sampler through numerical integration of the mean $\log L$ values collected over all of the chains. In the same way that inter-chain communication is hindered by phase transitions in the system, numerical estimation of this integral is susceptible to sharp changes in $\log L$ with the temperature T . Such phase transitions are marked by a diverging specific heat C_V since, from (3), C_V is the derivative of $\log L$ with respect to T .

Since allocating temperatures for uniform acceptance ratios yields a logarithmic chain density η that appears to scale with $\sqrt{C_V}$, such a temperature ladder will naturally increase the accuracy of numerical estimates of (25) with respect to one that does not increase η around phase transitions.

We can test the degree of improvement conferred by a uniform- A ladder by returning to the truncated Gaussian discussed in Section 4.1. Normalising (17) so that $\max \log L = 0$, the log evidence is

$$\begin{aligned} \Delta \log Z &= \left(\frac{\sqrt{2}}{R} \operatorname{erf} \left(\frac{R}{\sqrt{2}} \right) \right)^n \Gamma \left(1 + \frac{n}{2} \right) \\ &\approx -55.1, \end{aligned} \quad (26)$$

with $R = 30$ and $n = 25$.

Figure 21 illustrates the numerical estimates of $\Delta \log Z$ from a uniform- A ladder (with $T_{\max} = \infty$) and from geometric ladders with $T_{\max} = 10$ and $T_{\max} = 10^4$. The evidence quadratures for the geometric ladders are augmented with a copy of $\mathbb{E}[\log L]_{T_{\max}}$ placed at $T = \infty$ as a crude measure to cover the integration domain.

The evidence estimates recovered from these samplers are reported in Table 2 for 6 chains and 10, from which it is clear that selecting temperatures for uniform acceptance ratios can greatly increase the accuracy of the evidence estimate, bypassing the need to select a good initial temperature ladder. Note that the under- and over-estimates of $\Delta \log Z$ from the geometric ladders in this case are a consequence of poor choices of T_{\max} rather than of sharp changes in $\mathbb{E}[\log L]$. While these comparisons are reasonable – since for a geometric ladder it is very difficult to pick an appropriate T_{\max} in advance – we expect the presence of phase transitions to increase this disparity, and with it the advantages of adapting the ladder dynamically for uniform acceptance ratios.

6.3 Other measures of optimality

We have investigated the performance of a temperature ladder adapted for uniform acceptance ratios in reducing the

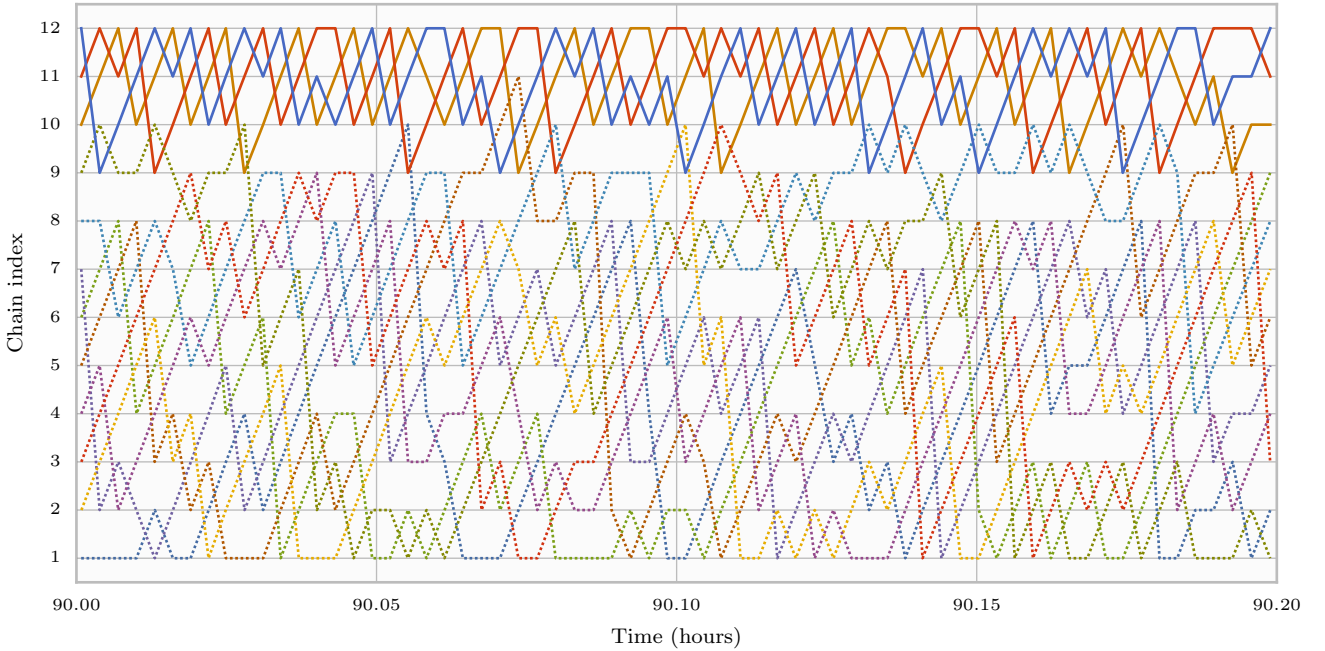


Figure 20. The paths traced out between temperatures by the 12 samples in a single-walker run with LALINFERENCE on a BNS signal of SNR 15. Samples are identified by their colour. While swap proposals between chains 9 and 10 are frequently accepted, there is no migration of samples starting above chain 10 (solid lines) to chains below 9, and vice versa (dotted lines).

Table 2. The evidence values of the truncated Gaussian of Section 4.1, estimated from a samplers of 6 and 10 temperatures allocated in three different ways, as compared to the analytical result.

Temperature ladder	$\Delta \log Z$	
	$N = 6$	$N = 10$
Uniform- A : $T_{\max} = \infty$	-58.0	-55.9
Geometric: $T_{\max} = 10^4$	-78.0	-61.8
Geometric: $T_{\max} = 10$	-42.3	-41.6
Analytical result	-55.1	

ACT of a parallel tempered MCMC sampler. The KL divergence discussed in Section 2.2 provides an alternative measure of the distance between two temperatures. In Section 4.1 we showed that uniform KL divergence in a temperature ladder does not correspond to uniform acceptance ratios beyond the special case of the ideal, unbounded Gaussian distribution described in Section 2.2.

When applied to the truncated Gaussian discussed in Section 4.1, for which $D_{\text{KL}}(\pi_{T_i} \parallel \pi_{T_{i+1}})$ is analytically available, the D_{KL} and A measured between chains drop off at different rates as T approaches T_{prior} (see Figure 5). Indeed, it is possible in principle to estimate the temperature-dependent normalising constants required to adapt on the KL divergence (Geyer 1994; Cameron & Pettitt 2014). It may be interesting to investigate such a scheme for resilience to the single-walker instability mentioned in Section 6.1.

Meanwhile, Katzgraber et al. (2006) propose an optimisation scheme in which temperatures are chosen to minimise the round-trip time of a sample from T_{\min} to T_{\max} ,

which they suggest will improve sampling performance on systems with strong phase transitions. Their algorithm is tested on simulations of the two-dimensional Ising model, and is shown to select a different temperature configuration than the uniform- A scheme that has been discussed so far.

However, the ACT of the sampler – what we are ultimately concerned with in efficient Bayesian inference – is not discussed, so it is unclear whether this strategy is better than selecting temperatures for uniform acceptance ratios. Their feedback optimisation method in fact prefers a higher density of chains per T across phase transitions of the system than the uniform- A scheme. We have shown, however, that the ACT yielded by a particular ladder is not critically sensitive to under-densities over phase transitions so long as the acceptance ratio is not prohibitively small in these temperature regimes (see Section 4.2.2). Indeed, increasing the density of chains over phase transitions too far might unnecessarily hinder inter-chain communication at other temperatures (by reducing A), leading to an overall rise in ACT.

These reservations, together with the complicated book-keeping involved in optimising for round-trip time, lead us to favour the dynamical method presented in Section 3. By comparison, this dynamical method is simple and guaranteed to produce an equilibrium ladder that yields efficient – if not perfectly optimal – sampling from any target distribution, with the proviso of many walkers per temperature.

ACKNOWLEDGEMENTS

We thank Ewan Cameron, Christopher Berry, and Daniel Foreman-Mackey for their critique and assistance. Figure 16

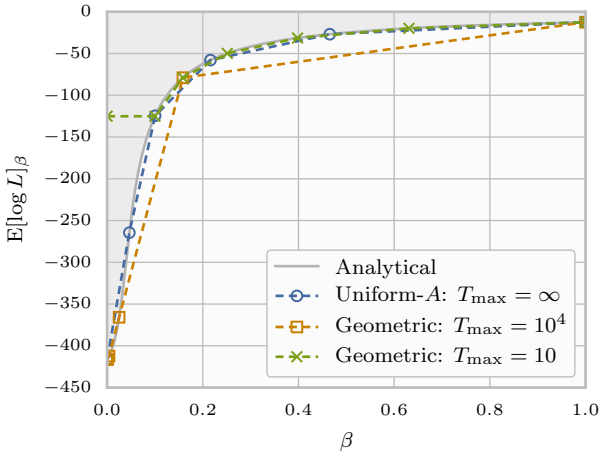


Figure 21. An illustration of the thermodynamic quadrature estimates of the log evidence of the truncated Gaussian discussed in Section 4.1. The shaded area shows the analytical mean log L as a function of β , while the dashed lines illustrate numerical approximations from the values of log L collected by samplers with different ladders, each of 6 temperatures. The resulting evidence estimates are reported in Table 2. Note the denser spacing of temperatures in the high-curvature region for the uniform- A ladder, and the errors incurred in extrapolating from T_{\max} to $T = \infty$ ($\beta = 0$) for the geometric ladders.

and Figure 17 were generated with TRIANGLE.PY (Foreman-Mackey et al. 2014). This work was supported by the Science and Technology Facilities Council and the Leverhulme Trust research project grant. We are grateful for computational resources provided by Cardiff University, and funded by an STFC grant supporting UK Involvement in the Operation of Advanced LIGO.

A reference implementation of the algorithm, based on the ensemble sampler EMCEE (Foreman-Mackey et al. 2013), is available at <https://github.com/willvousden/ptemcee>.

REFERENCES

- Aasi J., et al., 2013, *Phys. Rev. D*, **88**, 062001
Aasi J., et al., 2015, *Class. Quant. Grav.*, **32**, 074001
Abadie J., et al., 2010, *Class. Quant. Grav.*, **27**, 173001
Acernese F., et al., 2015, *Class. Quant. Grav.*, **32**, 024001
Buonanno A., Iyer B. R., Ochsner E., Pan Y., Sathyaprakash B. S., 2009, *Phys. Rev. D*, **80**, 084043
Cameron E., Pettitt A., 2014, *Statist. Sci.*, **29**, 397
Earl D. J., Deem M. W., 2005, *Phys. Chem. Chem. Phys.*, **7**, 3910
Falcioni M., Deem M. W., 1999, *J. Chem. Phys.*, **110**, 1754
Foreman-Mackey D., Hogg D. W., Lang D., Goodman J., 2013, *Pub. Astron. Soc. Pac.*, **125**, 306
Foreman-Mackey D., Price-Whelan A., Ryan G., Emily Smith M., Barbary K., Hogg D. W., Brewer B. J., 2014, triangle.py v0.1.1, doi:10.5281/zenodo.11020
Geyer C. J., 1991, in *Computing Science and Statistics, Proceedings of the 23rd Symposium on the Interface*. Interface Foundation of North America, New York, pp 156–163
Geyer C. J., 1994, Technical Report 568, Estimating normalizing constants and reweighting mixtures in Markov chain Monte Carlo, <http://purl.umn.edu/58433>. Univ. Minnesota, Minneapolis, <http://purl.umn.edu/58433>

- Goggans P. M., Chi Y., 2004, *AIP Conf. Proc.*, **707**, 59
Goodman J., Weare J., 2010, *Commun. Appl. Math. Comp. Sci.*, **5**, 65
Hannam M., Schmidt P., Bohé A., Haegel L., Husa S., Ohme F., Pratten G., Pürrer M., 2014, *Phys. Rev. Lett.*, **113**, 151101
Hukushima K., Nemoto K., 1996, *J. Phys. Soc. Jpn.*, **65**, 1604
Katzgraber H. G., Trebst S., Huse D. A., Troyer M., 2006, *J. Stat. Mech: Theory Exp.*, 2006, P03018
Kofke D. A., 2002, *J. Chem. Phys.*, **117**, 6911
Kofke D. A., 2004, *J. Chem. Phys.*, **120**, 10852
Lartillot N., Philippe H., 2006, *Syst. Biol.*, **55**, 195
Rathore N., Chopra M., de Pablo J. J., 2005, *J. Chem. Phys.*, **122**
Raymond V., van der Sluys M. V., Mandel I., Kalogera V., Röver C., Christensen N., 2010, *Class. Quant. Grav.*, **27**, 114009
Roberts G. O., Rosenthal J. S., 1998, *Can. J. Stat.*, **26**, 5
Roberts G. O., Rosenthal J. S., 2007, *J. App. Prob.*, **44**, 458
Rodriguez C. L., Farr B., Raymond V., Farr W. M., Littenberg T. B., Fazi D., Kalogera V., 2014, *Astrophys. J.*, **784**, 119
Sanbonmatsu K., García A., 2002, *Proteins: Struct., Funct., Bioinf.*, **46**, 225
Schug A., Herges T., Wenzel W., 2004, *Proteins: Struct., Funct., Bioinf.*, **57**, 792
Singer L. P., et al., 2014, *Astrophys. J.*, **795**, 105
Skilling J., 2006, *Bayesian Anal.*, **1**, 833
Sokal A., 1997, in DeWitt-Morette C., Cartier P., Folacci A., eds, NATO ASI Series, Vol. 361, *Functional Integration*. Springer US, pp 131–192, doi:10.1007/978-1-4899-0319-8_6
Sugita Y., Okamoto Y., 1999, *Chem. Phys. Lett.*, **314**, 141
Swendsen R. H., Wang J.-S., 1986, *Phys. Rev. Lett.*, **57**, 2607
The LIGO Scientific Collaboration 2010, LIGO Document T0900288-v3, Advanced LIGO anticipated sensitivity curves. The LIGO Scientific Collaboration
The Virgo Collaboration 2009, Virgo Technical Report VIR-0027A-09, Advanced Virgo Baseline Design. The Virgo Collaboration
Veitch J., Vecchio A., 2010, *Phys. Rev. D*, **81**, 062003
Veitch J., et al., 2015, *Phys. Rev. D*, **91**, 042003
Vitale S., Lynch R., Veitch J., Raymond V., Sturani R., 2014, *Phys. Rev. Lett.*, **112**, 251101
ter Braak C. J., Vrugt J. A., 2008, *Stat. Comput.*, **18**, 435
van der Sluys M., Raymond V., Mandel I., Röver C., Christensen N., Kalogera V., Meyer R., Vecchio A., 2008a, *Class. Quant. Grav.*, **25**, 184011
van der Sluys M. V., et al., 2008b, *Astrophys. J. Lett.*, **688**, L61

APPENDIX A: AUTOCORRELATION TIME ESTIMATION

The autocorrelation time (ACT) discussed in this paper refers to the *integrated autocorrelation time* described by Sokal (1997). It is estimated in the following way.

If $x(t)$ is a time series with a normalised autocorrelation function $\rho(t)$, such that $\rho(0) = 1$, then the integrated ACT of x is defined by

$$\begin{aligned}\tau &\equiv \sum_{t=-\infty}^{\infty} \rho(t) \\ &= 1 + 2 \sum_{t=1}^{\infty} \rho(t).\end{aligned}$$

Since, when $t \gg \tau$, $\rho(t) \approx 0$, there is little contribution to the integral at large lags, except through noise in the measured autocorrelation function ρ . We can therefore

approximate the ACT as

$$\tau \approx 1 + 2 \sum_{t=1}^{M\tau} \rho(t).$$

We estimate the ACT over a window that is $M = 5$ ACTs long, subject to the constraint that $M\tau < N/2$, where N is the number of samples in x . If this constraint is violated, the result is probably not trustworthy, since there are too few samples for a meaningful estimate.